Atmospheric Environment 145 (2016) 346–364

Contents lists available at ScienceDirect

Atmospheric Environment

journal homepage: www.elsevier.com/locate/atmosenv

A European aerosol phenomenology-5: Climatology of black carbon optical properties at 9 regional background sites across Europe

M. Zanatta [a, b, 1], M. Gysel [b, *], N. Bukowiecki [b], T. Müller [c], E. Weingartner [b, 2], H. Areskoug [d], M. Fiebig [e], K.E. Yttri [e], N. Mihalopoulos [f], G. Kouvarakis [f], D. Beddows [g], R.M. Harrison [g, h], F. Cavalli [i], J.P. Putaud [i], G. Spindler [c], A. Wiedensohler [c], A. Alastuey [j], M. Pandolfi [j], K. Sellegri [k], E. Swietlicki [l], J.L. Jaffrezo [a], U. Baltensperger [b], P. Laj [a, m]

[a] Univerisité Grenoble-Alpes, CNRS, Institut des Geosciences pour l'Environnement (IGE), Grenoble, France
[b] Laboratory of Atmospheric Chemistry, Paul Scherrer Institute, Villigen, CH-5232, Switzerland
[c] Leibniz Institute for Tropospheric Research (TROPOS), Permoserstrasse 15, 04318, Leipzig, Germany
[d] Atmospheric Science Unit, Department of Environmental Science and Analytical Chemistry (ACES), Stockholm University, Svante Arrhenius väg 8, SE-11418, Stockholm, Sweden
[e] NILU-Norwegian Institute for Air Research, Kjeller, Norway
[f] Environmental Chemistry Processes Laboratory, Dept. of Chemistry, University of Crete, 71003, Heraklion Crete, Greece
[g] National Centre for Atmospheric Science, School of Geography, Earth and Environmental Sciences, University of Birmingham, B15 2TT, UK
[h] Department of Environmental Sciences, Center of Excellence in Environmental Studies, King Abdulaziz University, PO Box 80203, Jeddah, 21589, Saudi Arabia
[i] European Commission, Joint Research Centre (JRC), Directorate for Energy, Transport and Climate, Air and Climate Unit, Via E. Fermi 2749, I-21027 Ispra (VA), Italy
[j] Institute of Environmental Assessment and Water Research (IDAEA-CSIC), c/ Jordi-Girona 18-26, ES08034, Barcelona, Spain
[k] Laboratoire de Météorologie Physique, UMR 6016, CNRS/University of Clermont-Ferrand, Clermont-Ferrand, France
[l] Division of Nuclear Physics, Department of Physics, Lund University, Lund, Sweden
[m] Division of Atmospheric Science, Department of Physics, University of Helsinki, P.O. Box 64, FIN-00014, Helsinki, Finland

HIGHLIGHTS

- The mass absorption cross-section of black carbon is homogeneous over Europe.
- Mass absorption cross-section of European black carbon is quantified in 10 m^2 g^{-1}.
- Presence of non-absorbing matter induces an enhancement of black carbon absorption.

GRAPHICAL ABSTRACT

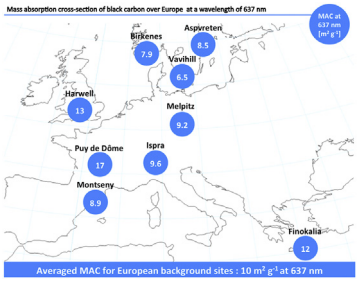

ARTICLE INFO

Article history:
Received 1 April 2016
Received in revised form
14 September 2016
Accepted 17 September 2016
Available online 18 September 2016

ABSTRACT

A reliable assessment of the optical properties of atmospheric black carbon is of crucial importance for an accurate estimation of radiative forcing. In this study we investigated the spatio-temporal variability of the mass absorption cross-section (MAC) of atmospheric black carbon, defined as light absorption coefficient (σ_{ap}) divided by elemental carbon mass concentration (m_{EC}). σ_{ap} and m_{EC} have been monitored at supersites of the ACTRIS network for a minimum period of one year. The 9 rural background sites

* Corresponding author.
E-mail address: martin.gysel@psi.ch (M. Gysel).
[1] Now at: Alfred Wegener Institute (AWI), Helmholtz Centre for Polar and Marine Research, Bremerhaven, Germany.
[2] Now at: Institute for Aerosol and Sensor Technology, University of Applied Sciences (FHNW), Windisch, Switzerland.

http://dx.doi.org/10.1016/j.atmosenv.2016.09.035

Keywords:
Black carbon
Europe
Mass absorption cross-section
MAC
Light absorption
Elemental carbon
Radiative forcing
Photometer
Thermal optical analysis
Atmosphere
ACTRIS
Ebas

considered in this study cover southern Scandinavia, central Europe and the Mediterranean. σ_{ap} was determined using filter based absorption photometers and m_{EC} using a thermal-optical technique. Homogeneity of the data-set was ensured by harmonization of all involved methods and instruments during extensive intercomparison exercises at the European Center for Aerosol Calibration (ECAC). Annual mean values of σ_{ap} at a wavelength of 637 nm vary between 0.66 and 1.3 Mm^{-1} in southern Scandinavia, 3.7–11 Mm^{-1} in Central Europe and the British Isles, and 2.3–2.8 Mm^{-1} in the Mediterranean. Annual mean values of m_{EC} vary between 0.084 and 0.23 $\mu g\ m^{-3}$ in southern Scandinavia, 0.28–1.1 in Central Europe and the British Isles, and 0.22–0.26 in the Mediterranean. Both σ_{ap} and m_{EC} in southern Scandinavia and Central Europe have a distinct seasonality with maxima during the cold season and minima during summer, whereas at the Mediterranean sites an opposite trend was observed. Annual mean MAC values were quite similar across all sites and the seasonal variability was small at most sites. Consequently, a MAC value of 10.0 $m^2\ g^{-1}$ (geometric standard deviation = 1.33) at a wavelength of 637 nm can be considered to be representative of the mixed boundary layer at European background sites, where BC is expected to be internally mixed to a large extent. The observed spatial variability is rather small compared to the variability of values in previous literature, indicating that the harmonization efforts resulted in substantially increased precision of the reported MAC. However, absolute uncertainties of the reported MAC values remain as high as ± 30–70% due to the lack of appropriate reference methods and calibration materials.

The mass ratio between elemental carbon and non-light-absorbing matter was used as a proxy for the thickness of coatings around the BC cores, in order to assess the influence of the mixing state on the MAC of BC. Indeed, the MAC was found to increase with increasing values of the coating thickness proxy. This provides evidence that coatings do increase the MAC of atmospheric BC to some extent, which is commonly referred to as lensing effect.

1. Introduction

Black carbon (BC) particulate matter, also commonly referred to as refractory carbon or elemental carbon, is emitted by incomplete combustion of fossil fuels and biomass (see Section 2.1 for details about the terminology for carbonaceous combustion particles). BC represents a small fraction of the European atmospheric aerosol, typically contributing less than 10% to the total mass concentration of particles in both size fractions smaller than 2.5 μm and 10 μm in diameter (Putaud et al., 2004; Yttri et al., 2007). Despite being a minor mass fraction only, it has been argued that anthropogenic BC might cause the second largest positive radiative forcing after CO_2 (Jacobson, 2001; Bond et al., 2013). This value is, however, associated with a high uncertainty (90%), resulting in an RF_{BC} range between 0.17 and 2.1 $W\ m^{-2}$ (Myhre et al., 2013). The calculation of RF_{BC} depends on the light absorption coefficient attributed to atmospheric particulate BC. The light absorption by BC is often inferred from measured or modeled BC mass concentrations using the mass absorption cross-section (MAC; see Equation (10) in Section 2.3.3). Thus, the estimated RF_{BC} is not only sensitive to the modeled BC mass concentration but also to the applied MAC value. Current state-of-the-art RF_{BC} estimates are based on a fixed MAC value without accounting for its spatio-temporal variability (Koch et al., 2009). However, the correct MAC value and its spatio-temporal variability remain poorly quantified, and thus could potentially lead to considerable uncertainty in the RF_{BC} assessment (Schulz et al., 2006; Koch et al., 2009).

Besides radiative forcing assessment, the MAC value is also required to infer the equivalent black carbon (eBC) mass concentration from measurements of the light absorption coefficient. Such observations are often used as reference data sets for the validation of models simulating atmospheric elemental carbon (EC) mass concentrations (e.g. Vignati et al., 2010). The eBC mass concentration is meant to be equal to the EC mass concentration as measured by thermal-optical methods (Petzold et al., 2013). However, this is only achieved under several conditions. First, the light absorption coefficient is measured for a wavelength at which EC causes virtually all light absorption (red to near-infrared). Second, the light absorption coefficient is correctly measured, which is generally challenging and even more for filter-based methods (see Section 2.3.2). Third, the true MAC value of the sampled aerosol is applied for the conversion of the light absorption coefficient to eBC mass concentration. The latter is a potential source for differences between eBC and EC mass concentrations because commercial instruments typically use a predefined fixed MAC value, which does often not agree with the MAC value of the sampled aerosol.

In Table 1 we report MAC values from the literature, which range between 4.3 and 22.7 $m^2\ g^{-1}$ at a wavelength of 637 nm. Part of this variability may be attributed to variability of the microphysical properties of BC-containing particles due different sources (e.g. Schwarz et al., 2008b; Martins et al., 1998) and/or differences in atmospheric aging processes during transport of BC to certain locations (Liousse et al., 1993; Cozic et al., 2008; Reche et al., 2011; Pandolfi et al., 2011, 2014; Genberg et al., 2013; Laborde et al., 2013). However, in this study we show that a substantial portion of this variability can also be attributed to experimental uncertainties, i.e. systematic biases of the methods applied to determine the MAC.

Sources and atmospheric aging processes define the properties of BC-containing particles to which the MAC is sensitive: index of refraction and material density of BC as well as particle size, shape and mixing with other particulate matter (Bond et al., 2013 and references therein). We can distinguish two different types of mixing: external mixture, in which case BC is present in pure form, i.e. BC is not mixed with other aerosol components in the same particle, and internal mixture, in which case BC is coated, i.e. BC is mixed with other aerosol components in the same particle. Freshly emitted BC can be externally or internally mixed, depending on its source. Atmospheric aging processes such as condensation, cloud processing or coagulation additionally transform externally mixed BC to internally mixed BC. Most BC becomes mixed with other components such as inorganic salts and acids or organic matter within 1–5 days (Jacobson, 2001; Riemer et al., 2010; Fierce et al., 2015) while in polluted urban areas BC becomes internally mixed within 12 h after emission (Moteki et al., 2007).

In general, it is accepted that internal mixing with non-

Table 1
Selected MAC values from the literature. The 2nd and 3rd column list the MAC values and corresponding wavelength as reported in the original literature. The 4th column lists the MAC values adjusted to 637 nm assuming an absorption Ångstrom exponent of 1.0.

Location	MAC [$m^2\ g^{-1}$]	Wavelength [nm]	MAC @ 637 nm [$m^2\ g^{-1}$]	Reference
Remote areas	5		4.3	
Mediterranean	18		15.5	
Savannah	20	550	17.3	Liousse et al., 1993
Urban	12		10.4	
Biomass burning (Brazil)	12.1	550	10.5	Martins et al., 1998
Urban	6.8–8.7	550	5.9–7.5	Hitzenberger et al., 2006
High altitude (winter)	7.6	630	7.5	Cozic et al., 2008
High altitude (summer)	11.1		11	
Traffic	9.1	530	7.6	Schwarz et al., 2008b
Biomass burning	13		10.8	
High altitude (spring)	10.2	630	10.1	Liu et al., 2010
Rural (Magadino)	14.4		14.9	
Rural (Magadino)	18.5	660	19.2	Herich et al., 2011
Urban (Zurich)	14.0		14.5	
Regional background (Montseny)	10.4	635	10.4	Pandolfi et al., 2011
Urban (Barcelona)			9.2	
Traffic (Bern)			10.3	Reche et al., 2011
Industrial (Huelva)			9.8	
Urban (Paris)	8.6	880	11.9	Laborde et al., 2013
Aspvreten	16.3		14.1	
Birkenes	25.9		22.4	
Harwell	9.14	550	7.9	Genberg et al., 2013
Melpitz	4.55		3.9	
Vavihill	26.2		22.7	
High altitude			10.9	Pandolfi et al., 2014

absorbing material induces an enhancement in the light absorption through the so-called lensing effect (e.g. Fuller et al., 1999; Bond et al., 2013) even though this enhancement effect is still debated (Cappa et al., 2012).

In this work, we investigate the spatio-temporal variability of the MAC. For this purpose, we use long-term data-sets from 9 supersites across Europe of the ACTRIS (Aerosols, Clouds, and Trace gases Research InfraStructure; http://www.actris.eu) research infrastructure, where more than 1 year of parallel light absorption coefficient and elemental carbon mass concentration measurements were available. A key feature of this data-set is its homogeneity, which is ensured with extensive instrument calibration and intercomparison exercises as part of the ACTRIS and ACTRIS-2 research infrastructure. Besides, this dataset provides evidence that the lensing effect increases the MAC of BC.

2. Method

2.1. Terminology

The terminology for describing various properties of carbonaceous particles emitted by incomplete combustion processes, casually referred to as soot particles, is ambiguous in the literature. Here we adopt the recent recommendations by Petzold et al. (2013). The term black carbon (BC) is used to refer, in a general sense, to the most refractory, insoluble and strongly light-absorbing component of combustion particles. BC is essentially elemental carbon (EC), i.e. almost pure carbon with a graphitic-like chemical microstructure. These features distinguish BC from organic carbon (OC), which is the other major component of carbonaceous combustion particles. The term BC-containing particle is used to refer to BC internally mixed with other particulate matter. More specific terms for BC are used whenever referring to BC properties in a quantitative manner. EC mass concentration (m_{EC}) is used for BC mass concentration measured by means of thermal-optical methods. Equivalent black carbon (eBC) is used whenever BC is indirectly quantified by inferring the eBC mass concentration (m_{eBC}) from light absorption coefficient (σ_{ap}) measurements. The attribute "equivalent" reflects the fact that a MAC value, MAC_{eBC}, needs to be assumed for calculating m_{eBC}:

$$m_{eBC} = \frac{\sigma_{ap}(\lambda)}{MAC_{eBC}(\lambda)} \quad (1)$$

Accordingly, m_{eBC} is only identical with m_{EC}, if the MAC value assumed for calculating m_{eBC} from σ_{ap} is equal to the true MAC value of the BC in the aerosol under consideration, as already mentioned in Section 1.

2.2. The ACTRIS sites

The present work is based on data recorded at atmospheric research supersites of the ACTRIS network. All data presented here were downloaded from the EBAS database (http://ebas.nilu.no/), developed and operated by the Norwegian Institute for Air Research (NILU). In order to ensure statistical robustness and coverage of a full seasonal cycle for every site, we set a minimal requirement of at least one year of simultaneous absorption coefficient and EC mass concentration measurements. Nine supersites satisfied this criterion: Aspvreten (APT), Birkenes (BIR), Finokalia (FKL), Harwell (HRL), Ispra (IPR), Melpitz (MEL), Montseny (MSY), Puy de Dôme (PUY) and Vavihill (VAV). Fig. 1 shows the geographical location of the supersites. They can be grouped into three different regions by latitude: Scandinavia, Central Europe and

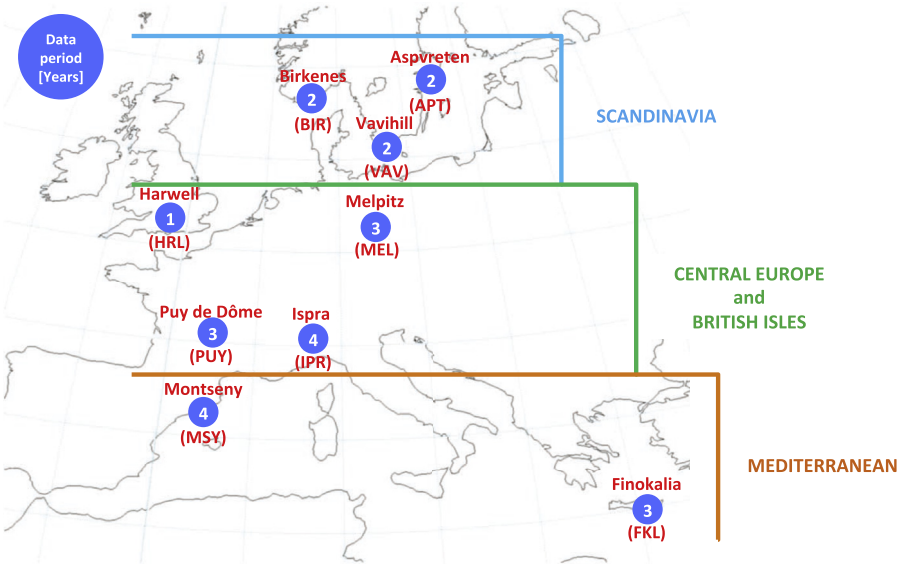

Fig. 1. Location of sampling sites and duration of measurements included in this study.

the British Isles, and the Mediterranean region. The main characteristics of each observation site, including instrumentation relevant to the present study, are summarized in Table 2. Additional details on the data availability for the considered sites are given in Table S1.

2.2.1. Scandinavia

The Aspvreten station (APT, Sweden, 58° 48′N, 17° 23′E, 30 m asl.) is operated by the Department of Environmental Science and Analytical Chemistry (ACES) of the Stockholm University. The station is located away from any local sources, placed in a boreal forest and is representative for the regional background. The Birkenes atmospheric research station (BIR, Norway, 58° 23′N, 8° 15′E, 190 m asl.) is run by the Norwegian Institute for Air Research (NILU), is located in the southern part of Norway, and is well suited to monitor long-range transported aerosol particles as it is far away from major anthropogenic sources. Vavihill (Sweden, VAV, 56° 01′N, 13° 09′E, 172 m asl.) is operated by Lund University. VAV is a background site with no local sources of pollution, situated in the southern-most part of Sweden.

2.2.2. Central Europe and the British Isles

The Harwell site (HRL, England, 51° 34′N, 1° 19′W, 60 m asl.) is operated by the University of Birmingham, primarily on behalf of the Department for Environment, Food and Rural Affairs (DEFRA). HRL is a rural station representative of large-scale air masses affecting Southern England with the occasional influence of London emissions. The Ispra atmospheric research station (IPR, Italy, 45° 49′N, 8° 38′E, 209 m asl.) is run by the Institute for Environment and Sustainability of the EC Joint Research Centre. Ispra is representative of the regional background at the southern edge of the Alps affected by pollution from the Po Valley. The TROPOS atmospheric research station Melpitz, (MEL, Germany, 51° 32′N, 12° 54′E, 87 m asl.) is operated by the Leibniz Institute for Tropospheric Research and represents a rural polluted continental site in Eastern Germany. The Puy de Dôme station (PUY, France, 45° 46′N, 2° 57′E, 1465 m asl.) is run by the "Observatoire de Physique du Globe" (OPGC) and by the "Laboratoire de Météorologie Physique" (LaMP) of the National Center for Scientific Research (CNRS). Despite the proximity of the urban area of Clermont-Ferrand, the latter has very little influence on the aerosol observed at PUY (Henne et al., 2010). Measurements at PUY are representative of the regional atmospheric background aerosol composition on synoptic scale distances.

Table 2
List of observatories included in the present study, as well as a description of measurement methodology and site characteristics. The sites are arranged in alphabetic order.

Site (country)		Station code	Coordinates	Altitude [m asl]	Period	Thermal protocol for m_{EC}	Instrument for σ_{ap} (wavelength)	Aerosol size fraction		Region
								m_{EC}	σ_{ap}	
Aspvreten	(SE)	APT	58° 48′ N, 17° 23′E	30	2010–2011	EUSAAR-2	PSAP-ITM (522 nm)	PM10	Total	Scandinavia
Birkenes	(NO)	BIR	58° 23′ N, 8° 15′ E	190	2010–2011	EUSAAR-2	PSAP-ITM (525 nm)	PM10	PM10	Scandinavia
Finokalia	(GR)	FKL	35° 20′ N, 25° 40′ E	250	2008–2010	EUSAAR-2	Aethalometer AE21 (880 nm)	PM10	Total	Mediterranean
Harwell	(GB)	HRL	51° 34′ N, 1° 19′ W	60	2010	NIOSH-like[a]	Aethalometer AE22 (880 nm)	PM10	Total	British Isles
Ispra	(IT)	IPR	45° 49′ N, 8° 38′ E	209	2008–2011	EUSAAR-2	MAAP (637 nm)	PM2.5	Total	Continental Europe
Melpitz	(DE)	MEL	51° 32′ N, 12° 54′ E	87	2008–2010	VDI-2465	MAAP (637 nm)	PM10	Total	Continental Europe
Montseny	(ES)	MSY	41° 46′ N, 2° 21′ E	720	2008–2011	EUSAAR-2	MAAP (637 nm)	PM10	PM10	Mediterranean
Puy de Dôme	(FR)	PUY	45° 46′ N, 2° 57′ E	1465	2008–2010	EUSAAR-2	MAAP (637 nm)	PM10	Total	Continental Europe
Vavihill	(SE)	VAV	56° 01′ N, 13° 09′ E	172	2010–2011	EUSAAR-2	PSAP-ITM (520 nm)	PM10	Total	Scandinavia

[a] NIOSH-like protocol alternatively named "QUARTZ" and described in (Yttri et al., 2009).

2.2.3. Mediterranean

The Finokalia station (FKL, Greece, 35° 20′N, 25° 40′E, 250 m asl.) is run by the Environmental Chemical Processes Laboratory (ECPL) of the University of Crete. The FKL station is located in the Southeastern Mediterranean, far from any local source of pollution and the observations are representative of the aged regional background aerosol of the Eastern Mediterranean Basin with the frequent influence of dust (Sahara) and sea-salt (Mediterranean Sea). The station of Montseny (MSY, Spain, 41° 46′N, 2° 21′E, 720 m asl.) belongs to the Air Quality Network of the Government of Catalonia and is run by the Institute of Environmental Assessment and Water Research (IDAEA-CSIC). MSY is a middle altitude emplacement located in the Montseny Natural Park 40 km NNE of the Barcelona urban area and 25 km from the Mediterranean coast. Such orography is typical for this region and the regional background aerosol encountered at Montseny is representative of the Western Mediterranean Basin with additional urban, sea salt or dust (Sahara) influence depending on meteorological conditions.

2.3. Experimental methods

The work performed in the present study is based on experimental data acquired at different stations using a range of different instruments and measurement protocols. Interpretation of spatial differences, reflecting the influence of the local environment and typical transport pathways influencing each site, is only possible if the data-set is homogeneous across all involved sites. The activities of the ACTRIS research infrastructure include considerable harmonization efforts such as extensive instrument intercomparison campaigns in order to minimize potential systematic differences between equal instrument types as well as between different instruments or protocols for measuring the same quantity. For this study, all σ_{ap} and m_{EC} measurements were harmonized to a common reference technique, as described in the following. The data reduction presented here maximizes the homogeneity of the whole data-set, whereas uncertainties of the absolute values remain, due to the lack absolute standards (Baumgardner et al., 2012).

2.3.1. Elemental carbon mass determination

A widespread approach to quantify OC and EC are thermal-optical techniques, which differentiate EC from OC through their thermal properties with optical correction for potential charring artefacts (Karanasiou et al., 2015). Most commonly applied temperature ramp protocols are NIOSH-5040 (Birch and Cary, 1996), QUARTZ (NIOSH-like; Yttri et al., 2009), IMPROVE (Chow et al., 2007), or EUSAAR-2 (Cavalli et al., 2010). Briefly, the aerosol is deposited on a quartz-fiber filter. The collected OC mass is then determined during a first desorption step in an inert atmosphere (He) at multiple medium-to-high temperatures starting at 140–310 °C and reaching up to 580–940 °C depending on the thermal protocol (NIOSH-5040, QUARTZ, IMPROVE-A or EUSAAR-2). The EC mass is then quantified during a second desorption step under oxidizing conditions (He/O_2 mixture) at multiple higher temperatures starting at 500–580 °C and reaching up to 840–890 °C depending on the thermal protocol. Temperature steps and analysis time for the most common thermal protocols are summarized in Karanasiou et al. (2015). All desorbed carbonaceous compounds are oxidized to CO_2, which is measured via non-dispersive infrared detection (Chow et al., 1993) or by flame ionization detection after reduction to methane (Birch and Cary, 1996). Ideally, all OC should be completely desorbed during the first inert atmosphere step, while EC should only be burned off in the second oxidizing step. However, some OC may be pyrolized and converted to EC during the first step, thereby systematically biasing the OC-EC discrimination (Huntzicker et al., 1982). Correction for this charring artefact is commonly done by estimating the contribution of the pyrolytic carbon to the carbon desorbed in the second step through continuous monitoring of the light transmittance through or light reflectance at the filter (Dod et al., 1979; Johnson and Huntzicker, 1979), which is referred to as thermal-optical transmittance (TOT) or thermal-optical reflectance (TOR) method, respectively. Previous inter-laboratory and inter-protocol comparison studies revealed a good agreement in the total carbon (TC) mass concentration, whereas substantial systematic differences are observed in discriminating between the OC and EC fractions between different temperature protocols, between TOT and TOR with equal temperature protocol as well as between individual instruments applying the same protocol (Chiappini et al., 2014; Cavalli et al., 2016).

In this study, we choose the EUSAAR-2 protocol with light transmission for charring correction (TOT), which has been selected as the standard method for the ACTRIS research infrastructure, as our basis for determining the EC mass concentrations, from which the MAC are calculated. Homogeneity of the EC data from sites that apply the EUSAAR-2 protocol is maximized by instrument specific harmonization factors to correct for systematic instrument-to-instrument variability. EC data from sites that apply a different protocol or approach are adjusted with correction factors, in order to make them equivalent to EUSAAR-2 based data.

A schematic of the data analysis and harmonization approach applied in this study is provided in Fig. 2. Raw EC mass concentrations ($m_{EC,raw}^{TOT}$), which are already corrected for the charring artefact, were provided by the observatories. Final harmonized EC mass concentration (m_{EC}) were then obtained by applying instrument-specific harmonization factors (HF_{EC}):

$$m_{EC} = \frac{m_{EC,raw}^{TOT}}{HF_{EC}} \quad (2)$$

The harmonization factors were determined by Cavalli et al. (2016) for all thermal-optical instruments applied at observatories of the ACTRIS research infrastructure as part of an intense intercomparison exercise. Identical samples, i.e. filter punches from the same filter, were analyzed by all instruments. This was done for a series of randomly chosen filters. The reference value, m_{EC}^{ref}, for the EC mass on each test filter was then defined to be the average of all raw EC mass values from those instruments that apply the EUSAAR-2 protocol. The harmonization factor for each instrument is then set equal to $m_{EC,raw}^{TOT}$ measured by this particular instrument divided by the reference value m_{EC}^{ref} (after averaging both over all test filters). As a consequence, the final harmonized EC measurements, m_{EC}, become by definition equal to the reference value, when again considering the average over all test filters. This harmonization procedure ensures the homogeneity of the EC mass concentration data-set from the different sites by minimizing potential differences arising from instrument to instrument variability as well as differences in the measurement protocol. The importance of the intercomparison and harmonization efforts is reflected in the fact that the harmonization factors, which are listed in Table 3, span a considerable range from 0.74 to 1.35 even for those seven sites where the identical EUSAAR-2 protocol is applied (Table 2).

At Harwell, the NIOSH-like protocol “QUARTZ” with light transmission for charring correction is applied (Yttri et al., 2009; Querol et al., 2013; we will refer to it as “NIOSH-like”). The temperature ramp of this thermal-optical protocol deviates slightly from that of the EUSAAR-2 protocol. Thus, the results of this instrument were not included in calculating m_{EC}^{ref} of the inter-laboratory comparisons, whereas the harmonization factor was also determined against m_{EC}^{ref} and applied in the same manner (Equation (2)). Using this approach, the final harmonized EC mass from the NIOSH-like method become equivalent to EUSAAR-2

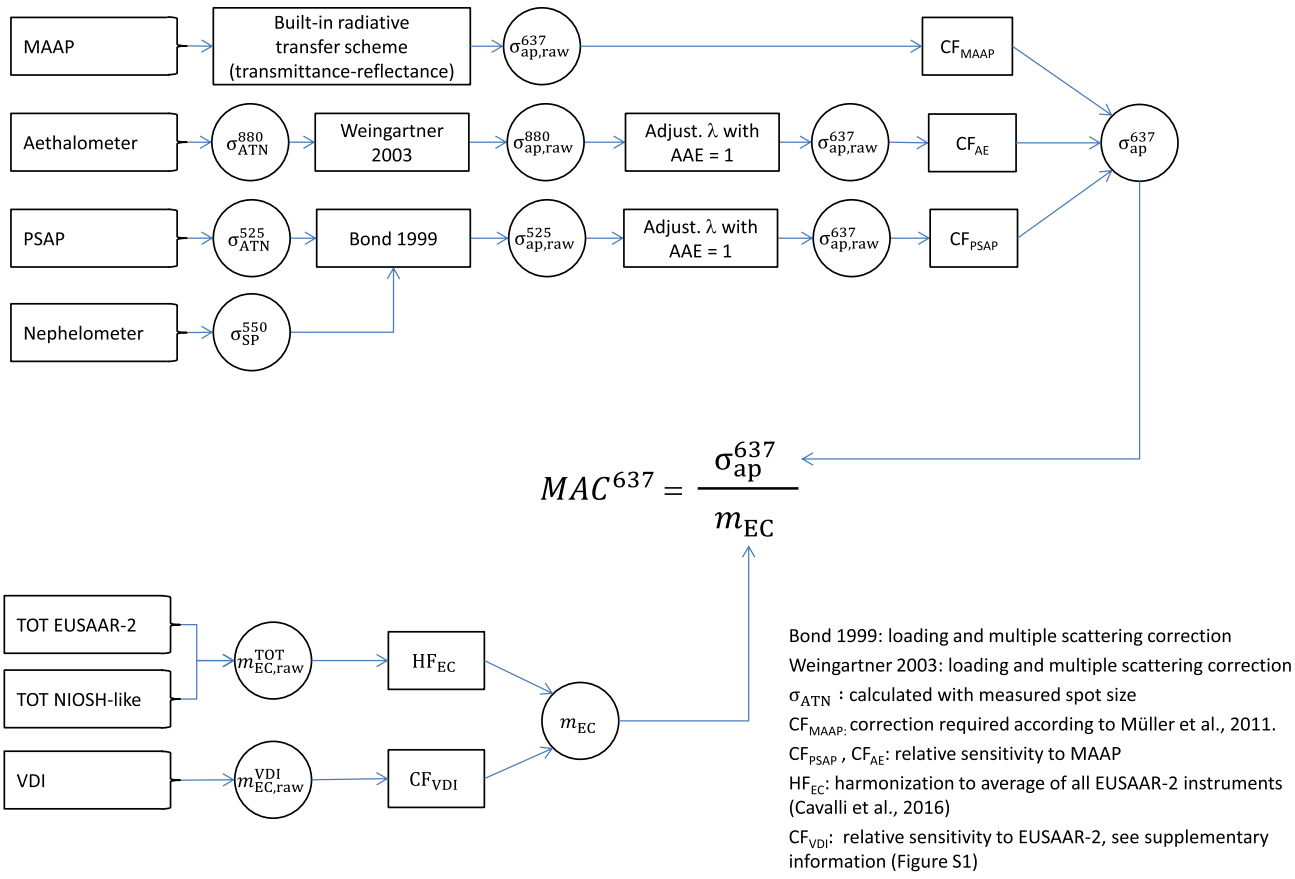

Fig. 2. Flowsheet of how to obtain corrected and harmonized EC mass concentrations (m_{EC}) and absorption coefficients (σ_{ap}^{637}) from the raw data delivered by different types of instruments and methods, which are then used to calculate the mass absorption cross-section values for a wavelength of 637 nm (MAC^{637}). Details are provided in Section 2.3 and in the supplementary information.

Table 3
Harmonization and correction factors applied in the data analysis as described in Section 2.3. HF_{EC}, which was determined by Cavalli et al. (2016) during extensive inter-comparison exercises, is an instrument specific harmonization factor to correct for systematic differences between the individual thermal-optical instruments with respect to the average of all EUSAAR-2 instruments. The range of values required to correct the thermal EC measurements at Melpitz is listed under CF_{VDI}[a]. CF_{MAAP} is the correction factor applied to the firmware output from the MAAP (Müller et al., 2011). D_{spot} is the measured spot diameter that was applied in the initial data analysis steps for the PSAP and aethalometer instruments. K_1 and K_2 are the coefficients that have been applied to the PSAP data following the Bond correction (Bond et al., 1999). CF_{PSAP} is a correction factor to harmonize PSAP results with MAAP measurements (from a yet unpublished intercomparison workshop). f and C_{def} are the coefficients for loading and multi-scattering correction as applied using the approach by Weingartner et al. (2003). CF_{AE}[b] is a correction factor to harmonize the aethalometer results with MAAP measurements (Müller et al., 2011; WMO, 2016). α_{ap} is the absorption Angström exponent applied to adjust the absorption coefficients determined by aethalometer and PSAP to the wavelength of the MAAP.

Site	HF_{EC}	CF_{VDI}[a]	CF_{MAAP}	K_1	K_2	CF_{PSAP}	D_{spot} [mm^2]	f	C_{def}[b]	CF_{AE}[b]	α_{ap}
Aspvreten	1.35	n.a.	n. a.	0.02	1.22	1.59	7.07[c]	n. a.	n. a.	n. a.	1.0
Birkenes	1.02	n.a.	n. a.	0.02	1.22	1.94	11.3[c]	n. a.	n. a.	n. a.	1.0
Finokalia	1.19	n.a.	n. a.	n. a.	n. a.	n. a.	42.6[c]	1.1	2.14	1.64	1.0
Harwell	1.45	n.a.	n. a.	n. a.	n. a.	n. a.	150[c]	1.1	2.14	1.64	1.0
Ispra	0.93	n.a.	0.952	n. a.	n. a.	n. a.	n. a.	n. a.	n. a.	n. a.	n.a.
Melpitz	n.a.[a]	1.36–3.14[a]	0.952	n. a.	n. a.	n. a.	n. a.	n. a.	n. a.	n. a.	n.a.
Montseny	0.97	n.a.	0.952	n. a.	n. a.	n. a.	n. a.	n. a.	n. a.	n. a.	n.a.
Puy de Dôme	1.23	n.a.	0.952	n. a.	n. a.	n. a.	n. a.	n. a.	n. a.	n. a.	n.a.
Vavihill	0.74	n.a.	n. a.	0.02	1.22	2.20	7.30[d]	n. a.	n. a.	n. a.	1.0

[a] The thermal EC measurements made at Melpitz using the VDI method were adjusted to EC mass concentrations that are equivalent to values that would have been measured by a TOT-EUSAAR2 method. This was done by means of monthly mean corrections factors (Fig. S1).
[b] Applying $C_{def} = 2.14$ and $CF_{AE} = 1.64$ for inferring the absorption coefficient from the attenuation coefficient measured by the aethalometer is equal to simply applying a C-value of 3.5 for the multi-scattering correction in the approach by Weingartner et al. (2003) without any further corrections (except for the loading correction using the indicated f-value).
[c] Spot area as measured.
[d] Spot area as provided in Krecl et al. (2007).

based EC mass.

The harmonization is somewhat more complex at Melpitz, where a modified VDI thermal method without optical charring correction was applied (Cachier et al., 1989). This protocol is known to have a considerable high bias in the EC mass concentration measurement, which also depends considerably on aerosol

composition. Therefore, a full year comparison of EC measurements using both the VDI and the EUSAAR-2 protocols in parallel was performed at Melpitz in 2012. Figure S1 shows that the monthly mean ratio of the EC mass concentration measured by the two methods varies between 1.36 and 3.14 with a distinct seasonal pattern. We used the results of this comparison in 2012 to adjust the EC measurements, $m_{EC,raw}^{VDI}$, done at Melpitz from 2008 to 2010 in order to obtain EUSAAR-2 equivalent EC mass values. The adjustment of $m_{EC,raw}^{VDI}$ was done by correcting with the monthly mean CF_{VDI} from the corresponding month of the year, which is taken from Figure S1. This approach accounts for the seasonal pattern of the VDI to EUSAAR-2 ratio as well as possible. No harmonization of the thermal-optical EC instrument, which was used to determine CF_{VDI} at Melpitz, against the EUSAAR-2 reference, was done, as the uncertainty associated with the correction factor CF_{VDI} is the dominating source of error. In the meantime the thermal-optical instrument of TROPOS used for Melpitz samples took part at European inter-comparison exercises in 2014 and 2015 successfully.

2.3.2. Absorption coefficient measurement and data analysis approach

The absorption coefficient was measured using one of the following three filter based absorption photometer types (see Table 2): the Multi Angle Absorption Photometer (MAAP, Thermo Fisher Scientific, Waltham, USA), the Aethalometer AE22 model (Magee Scientific, Berkeley, USA) or the custom made Particle Soot Absorption Photometer (PSAP-ITM). These are all filter-based methods, i.e. the aerosol sample is being continuously collected on the filter except during filter changes. The primary measurement is the rate of change of light transmittance through the filter per deposited sample air volume unit, from which the attenuation coefficient is inferred (Weingartner et al., 2003). Quantitatively relating the absorption coefficient of an aerosol sample to its attenuation coefficient after deposition on the filter is mainly complicated by multiple scattering and "shadowing" effects (see e.g. Weingartner et al., 2003). First, the light attenuation coefficient of the particulate matter deposited on the filter is considerably larger than the corresponding absorption coefficient of the same amount of particulate matter in the form of an aerosol due to multiple scattering of light in the filter fibers. Second, the ratio of absorption coefficient to attenuation coefficient depends on the filter loading, as particles deposited deeper in the filter are shadowed by those deposited higher up in the filter. These two effects are accounted for with correction approaches. However, absorption coefficient measurements done with filter based methods always remain tainted with potentially substantial uncertainties. The MAAP, which has the most sophisticated measurement setup, has been shown to have the best accuracy (Petzold et al., 2005; Slowik et al., 2007; Moosmüller et al., 2009) among the instruments applied in the current study and it showed high agreement with an independent reference method which determines the absorption coefficient from the difference of light extinction minus scattering (Petzold et al., 2005). Therefore, we choose the absorption coefficients measured by the MAAP as a basis for calculating the MAC. Method specific correction factors are applied to the data from those sites operating a PSAP or an aethalometer to make them equivalent to MAAP based measurements and with that also as accurate as possible with available means. A schematic of the applied data analysis and correction procedures, which will be described in the following, is provided in Fig. 2 and all relevant data analysis parameters and correction factors are listed in Table 3.

Petzold and Schönlinner (2004) provided a detailed description of the MAAP instrument and data analysis approach. Briefly, it measures light transmittance in orthogonal direction through the filter as well as back-reflectance at two different angles. The firmware includes a full data inversion, which is based on a radiative transfer model, to directly infer the absorption coefficient ($\sigma_{ap,raw}^{637}$), whereby the reflectance signals provide the information required to account for the effects of multiple scattering and shadowing. Originally, the operating wavelength of the MAAP was thought to be 670 nm (Petzold et al., 2005), however, the true value was later shown to be 637 ± 1 nm. As a consequence of this, the absorption coefficient ($\sigma_{ap,raw}^{670}$) determined by the firmware of the MAAP needs to be increased by 5% assuming an Ångström exponent of 1 (Petzold et al., 2005) to obtain the correct aerosol absorption coefficient (σ_{ap}^{637}) at 637 nm (Müller et al., 2011):

$$\sigma_{ap}^{637} = \frac{\sigma_{ap,raw}^{670}}{CF_{MAAP}} \tag{3}$$

We applied this correction with $CF_{MAAP} = 0.952$ to the MAAP measurements used for this study, whereby the $\sigma_{ap,raw}^{670}$ was first calculated by multiplying the BC mass concentration output of the MAAP with 6.6 $m^2\ g^{-1}$ (this is the MAC applied within the MAAP firmware to convert between measured absorption coefficient and reported BC mass concentration; Nordmann et al., 2013).

The Aethalometer, model AE-22, measures the light transmission through the sample filter at 370 and 880 nm (Hansen et al., 1984). For the purpose of this study, we only used the 880 nm channel because light absorption by atmospheric aerosols in the near-infrared wavelength range is fully dominated by black carbon, as opposed to the near ultraviolet range, where organic matter may contribute substantially (Kirchstetter et al., 2004). A multi-step data analysis and correction procedure was applied to obtain an absorption coefficient at 637 nm (Fig. 2) that is equivalent to MAAP measurements. In a first step, the raw absorption coefficient at 880 nm ($\sigma_{ap,raw}^{880}$) is derived from the attenuation coefficient at 880 nm (b_{ATN}^{880}) reported by the instrument using the approach from Weingartner et al. (2003):

$$\sigma_{ap,raw}^{880} = \frac{b_{ATN}^{880}}{C_{def} R(ATN,f)} \tag{4}$$

where C_{def} is the factor to correct for multiple scattering effects and $R(ATN,f)$, which depends on the filter loading, accounts for the shadowing effect. In the initial data analysis step to infer the raw absorption coefficient $\sigma_{ap,raw}^{880}$ (Equation (4)), we chose a "default" value of $C_{def} = 2.14$ for the multi-scattering correction. The shadowing correction $R(ATN,f)$ is of the form:

$$R(ATN,f) = (1/f - 1)[ln(ATN) - ln(0.1)]/[ln(0.5) - ln(0.1)] + 1 \tag{5}$$

where ATN is the additional attenuation by adding particles to a blank filter. f is a parameter that mainly depends on the single scattering albedo of aerosol. Because no suitable simultaneous scattering coefficient measurements were available, we simply chose a fixed value of $f = 1.1$, which is between typical values for aged BC ($f = 1.025$) and freshly emitted BC ($f = 1.2$) (Collaud Coen et al., 2010). In order to verify the reliability of the shadowing correction for the chosen f value, the inferred raw absorption coefficients ($\sigma_{ap,raw}^{880}$) observed at the highest and lowest filter loadings, i.e. just before and after the filter change, respectively, were compared against each other. The fact that they differ as little as 0.18% and 0.28% for the Harwell and Finokalia data-sets, respectively, indicates that on average the shadowing effect is correctly accounted for.

In the next step, the raw absorption coefficient ($\sigma_{ap,raw}^{880}$), which was inferred from measurements at 880 nm, is adjusted to a raw

absorption coefficient ($\sigma^{637}_{ap,raw}$) at the wavelength of the MAAP (637 nm). This is done with the common approach to assume a constant absorption Ångström exponent (AAE; e.g. Lack and Langridge, 2013 and reference therein):

$$\sigma_{ap}^{\lambda_2} = \sigma_{ap}^{\lambda_1}\left(\frac{\lambda_1}{\lambda_2}\right)^{AAE} \quad (6)$$

Where λ_1 and λ_2 are the wavelengths 880 nm and 637 nm, respectively, and the AAE is assumed to be unity (AAE = 1.0).

So far, the wavelength-adjusted absorption coefficient, $\sigma^{637}_{ap,raw}$, was calculated with applying a legacy value of $C_{def} = 2.14$ for the multi-scattering correction (Weingartner et al., 2003). However, Collaud Coen et al. (2010) found, by relating aethalometer measurements of the absorption coefficient to parallel MAAP measurements, that *C*-values in the range between 2.9 and 4.3 are more realistic for atmospheric aerosols. The latest recommendation, which is based on further yet unpublished intercomparison of parallel aethalometer and MAAP measurements of atmospheric aerosols (Müller at al., in preparation), is to apply a *C*-value 3.5 for atmospheric aerosols (WMO, 2016). In order to derive MAAP-equivalent and accurate absorption coefficients we had to apply another correction to the aethalometer data

$$\sigma_{ap}^{637} = \frac{\sigma_{ap,raw}^{637}}{CF_{AE}} \quad (7)$$

with $CF_{AE} = 1.64$. Note that the product of C_{def} (2.14) and CF_{AE} (1.64) equals 3.5. Thus, our two step correction approach, which was chosen for legacy reasons and also to show how different *C*-values and correction factors are related to each other, is identical to directly applying a *C*-value of 3.5 for the multiple-scattering correction in the Weingartner et al. (2003) approach. Applying a correction of $CF_{AE} = 1.64$ is also in agreement with Müller et al. (2011), who reported a correction factor of $CF_{AE} = 1.6$ for aethalometer data analyzed with the "default" *C*-value of $C_{def} = 2.14$. No further efforts to minimize instrument-to-instrument variability were made, as the *C*-value is the dominant source of uncertainty (Section 2.3.4).

Custom made Particle Soot Absorption Photometers (PSAP-ITM) were installed at the Aspvreten, Birkenes, and Vavihill sites, operating at wavelengths of 522, 525, and 520 nm, respectively (Table 2). This instrument was developed by the Department of Applied Environmental Science at Stockholm University (ITM) and a full description of it is given in Krecl et al. (2007). It is similar to the commercial PSAP, which is described in detail in Bond et al. (1999). The latter study also provides a data correction approach, which is compatible with the data from the custom made PSAP-ITM. A first element of the Bond correction is to correct the instrument output for systematic deviations of the flow rate and spot size used in the firmware from their respective true values in order to obtain unbiased attenuation coefficients (σ^{525}_{ATN}). We simply used the standard correction factors as they are always applied for these three instruments (Table 3). The second and main element of the Bond correction is to derive the raw absorption coefficient from the attenuation coefficient:

$$\sigma_{ap,raw}^{525} = \frac{\sigma_{ATN}^{525} - K_1\sigma_{sp}}{K_2} \quad (8)$$

where σ_{sp} denotes the scattering coefficient of the aerosol. The term $K_1\sigma_{sp}$ accounts for misinterpretation of particle scattering as absorption and K_2 corrects for multiple scattering. We applied the Bond correction using the related correction coefficients $K_1 = 0.02$ and $K_2 = 1.22$, which are determined for the commercial PSAP but previously applied to PSAP-ITM data Müller et al. (2011), and with using scattering coefficients simultaneously measured at these sites by nephelometers. In the next step, the raw absorption coefficient measured by the PSAP-ITM ($\sigma^{525}_{ap,raw}$) at a wavelength of 525 nm (520 nm for Vavihill), was adjusted to the wavelength of the MAAP, which then provides the raw absorption coefficient at 637 nm ($\sigma^{637}_{ap,raw}$). This was done in the same manner as for the aethalometer data, i.e. by using Equation (6) and assuming an absorption Ångström exponent of unity (AAE = 1.0).

Recent intercomparison (unpublished) between MAAP and ITM-PSAP from Aspreveten, Birkenes and Vavihill revealed that absorption coefficients, $\sigma^{637}_{ap,raw}$, measured by the PSAP-ITM, analyzed with the Bond correction and parameters of the commercial PSAP, were systematically larger than those determined with MAAP. In order to derive MAAP-equivalent and accurate absorption coefficients, σ^{637}_{ap}, we applied another correction to the PSAP-ITM data:

$$\sigma_{ap}^{637} = \frac{\sigma_{ap,raw}^{637}}{CF_{PSAP}} \quad (9)$$

with $CF_{PSAP} = 1.59$ for the instrument operated at Aspvreten, $CF_{PSAP} = 1.94$ for the Birkenes instrument and $CF_{PSAP} = 2.2$ for the Vavihill (Table 3). The large values of CF_{PSAP} indicate that at least one instrument parameter of the commercial PSAP is not applicable to the PSAP-ITM instruments. However, the resulting systematic bias in $\sigma^{637}_{ap,raw}$ is eliminated from the final corrected values through applying the correction factors CF_{PSAP} (Equation (9)). Note, the above correction factors CF_{PSAP} are valid for PSAP-ITM raw absorption coefficients analyzed with the Bond correction and parameters of the commercial PSAP. Applying the more recent Ogren correction (Ogren, 2010) instead of the Bond correction to the ITM-PSAP data would change the resulting raw absorption coefficients slightly. However, the final corrected values would remain unchanged because such a systematic change of the raw values would also cause a counteracting change of the correction factors CF_{PSAP}.

2.3.3. Mass absorption cross-section (MAC)

The mass absorption cross-section (MAC^{λ}; [$m^2\ g^{-1}$]) of BC at a certain wavelength (λ) is defined as the ratio of the aerosol absorption coefficient (σ^{λ}_{ap}; [Mm^{-1}]) at this wavelength to the mass concentration (m_{EC}; [$\mu g\ m^{-3}$]) of the BC:

$$MAC^{\lambda} = \frac{\sigma_{ap}^{\lambda}}{m_{EC}} \quad (10)$$

Note that this simplified definition is only valid for wavelengths at which the light absorption is dominated by black carbon (see Section 2.3.4). We used the absorption coefficients and EC mass concentrations including all adjustments and corrections as detailed in Sections 2.3.1 and 2.3.2, respectively, for calculating the MAC values. The filter samples for the EC analysis were collected for 24 h at the Mediterranean, Central Europe and the British Isles sites and, due to lower aerosol loadings, for 3–7 days at the Scandinavian sites. The measured absorption coefficients, which are available at higher time resolution (≤1 h), were averaged over the time intervals of the filter sample, in order to obtain matching pairs of σ^{637}_{ap} and m_{EC}, before calculating the corresponding MAC values. In order to minimize the influence of outliers on the statistical analysis, all data below or above the 5th or 95th percentile, respectively, were filtered. This trimming has little effect on the geometric mean values (less than 5% difference) but it reduces the resulting geometric standard deviation values considerably.

2.3.4. Uncertainty estimates

The uncertainty estimates for reported EC mass, light absorption coefficient, and MAC values are summarized in Tables 4–6 respectively. The harmonization procedure applied to EC measurements and described in Section 2.3.1 increases the reproducibility of the reported EUSAAR-2 equivalent EC mass concentrations and contributes to the spatial homogeneity of the data-set. The 1σ reproducibility of the harmonized EUSAAR-2 EC mass concentration measurements is estimated to be $\Delta m_{EC}^{EUSAAR2} \approx \pm 24\%$ for the sites adopting the EUSAAR-2 protocol (see Table 4). This uncertainty accounts for contributions from three independent random errors: the residual uncertainty of single harmonized $EC_{EUSAAR2}$-to-TC ratios obtained from a certain instrument for samples included in the intercomparison (~±20%; Cavalli et al., 2016), the extra uncertainty introduced by applying the harmonization factors to samples that were not included in the intercomparison exercise (~±10%), and the uncertainty of TC mass concentration (~±10%). The reproducibility is poorer for the EUSAAR-2 equivalent EC mass data from the Harwell site ($\Delta m_{EC}^{NIOSH-like} \approx \pm 52\%$), as the harmonization factor is more uncertain, i.e. the ratio of NIOSH-like to EUSAAR-2 derived EC mass concentrations is more variable for different aerosol types (Cavalli et al., 2016). For Melpitz, using the modified thermal VDI protocol, the reproducibility is estimated to be $\Delta m_{EC}^{VDI} \approx \pm 55\%$, mainly limited by the uncertainty of the monthly mean harmonization factors.

The accuracy of thermal-optical EC measurements always remains limited due to the lack of a reference method or suitable standards (Baumgardner et al., 2012). Here we simply define the EC mass from measurements by EUSAAR-2 instruments as the "true" value. Consequently, systematically different EC mass values would have been obtained if choosing a different protocol as reference. For example choosing NIOSH-5040 as reference method would provide EC mass values that are systematically lower by ~40% (Piazzalunga et al., 2011; Maenhaut and Claeys, 2012); (see also Table 4). In a similar manner using the IMPROVE-A protocol with using light-transmission for charring correction as EC mass reference, would have resulted in positive systematic biases of 10–20% (Piazzalunga et al., 2011; Wu et al., 2012).

The MAAP is expected to provide the absorption coefficient at 637 nm with an accuracy of $\Delta\sigma_{ap}^{MAAP} \approx \pm 15\%$ (Petzold et al., 2005; Müller et al., 2011), which directly applies to the reported absorption coefficients. The major uncertainty of the absorption coefficient measured by the aethalometer arises from the multi-scattering correction, since the *C*-value varies by about ±25% (1σ)

Table 4
Uncertainty estimates of harmonized EUSAAR-2 and EUSAAR-2 equivalent EC mass concentration as discussed in Section 2.3.4.

Uncertainties of EC mass concentration (Δm_{EC}):	EUSAAR-2	NIOSH-like (Harwell)	VDI 2465 (Melpitz)
1σ reproducibility of the harmonized EUSAAR-2 or EUSAAR-2 equivalent EC mass. Valid if EUSAAR-2 is defined to be the reference method providing the true EC mass.	±24% [a]	±52%[a]	±55% [a]
Approximate systematic decrease of m_{EC} if the NIOSH-5040 protocol would have been used as reference method instead of EUSAAR-2[b]	-~ 40%	-~ 40%	-~ 40%
Approximate systematic decrease of m_{EC} if the IMPROVE-A protocol would have been used as reference method instead of EUSAAR-2[c]	+ ~15%	+~15%	+~15%

[a] This 1σ reproducibility accounts for contributions from three independent random errors: the residual uncertainty of single harmonized $EC_{EUSAAR2}$-to-TC ratios obtained from a certain instrument for samples included in the intercomparison (Cavalli et al., 2016), the extra uncertainty introduced by applying the harmonization factors to samples that were not included in the intercomparison exercise, and the uncertainty of TC mass concentration. The individual components contributing to the combined uncertainty are estimated to be ±20% plus ±10% plus ±10%, ±50% plus ±10% plus ±10%, and ±54% plus ±0% plus ±10% for measurements based on the EUSAAR2, Niosh-like (Harwell), and VDI 2465 (Melpitz) protocols, respectively.
[b] Estimated from Piazzalunga et al. (2011) and Maenhaut and Claeys (2012).
[c] Estimated from Piazzalunga et al. (2011) and Wu et al. (2012).

Table 5
Uncertainty estimates of corrected absorption coefficients for the wavelength 637 nm as discussed in Section 2.3.4.

Uncertainties of absorption coefficient ($\Delta\sigma_{ap}^{637}$):	MAAP	Aethalometer	PSAP-ITM
Wavelength of the absorption coefficient measurement.	637 nm	880 nm	520-525 nm
1σ accuracy of reported total absorption coefficient σ_{ap}^{637}	±15%	±35%	±25%
Potential maximal systematic bias in total absorption coefficient reported at 637 nm due to assuming AAE = 1 for the wavelength adjustment for aerosols types that contain light-absorbing organic matter. (positive value means that true total absorption would be higher than reported total absorption)	0%	+10%[a]	−20%[b]
Potential maximal interference in true total absorption coefficient from light-absorbing organic matter. The negative value indicates how much smaller the true absorption from BC alone would be relative to true total absorption.	−10%[c]	−10%[c]	−10%[c]
Potential maximal systematic difference between reported total absorption coefficient and true absorption coefficient from BC alone at a wavelength of 637 nm for aerosols that contain light-absorbing organic matter (this is the sum of the above two lines). (negative value means that true absorption from BC alone is smaller than reported total absorption)	−10%	0%[d]	−30%

[a] If the AAE of the ambient aerosol was 1.3 instead of 1.0 for the wavelength pair 637/880 nm.
[b] If the AAE of the ambient aerosol was 2.0 instead of 1.0 for the wavelength pair 525/637 nm.
[c] This systematic bias corresponds to an increase of the ambient aerosol AAE for the wavelength pair 637/880 nm from 1.0 without organic interference to 1.3 with organic interference (and the implicit assumption that no organic interference occurs at 880 nm).
[d] No systematic from organic interference occurs in the absorption coefficient of BC determined with the Aethalometer as the measurement is taken at a wavelength of 880 nm, at which absorption by organics is negligible. Consequently, the systematic errors in the two rows above must cancel each other for the aethalometer results, if assumptions about organic interference are made in a consistent manner.

Table 6
Uncertainty estimates of reported mass absorption cross-section values for a wavelength of 637 nm (ΔMAC^{637}) as obtained by propagating the uncertainties listed in Tables 4 and 5 through Equation (10).

Uncertainties of MAC (ΔMAC^{637}):					
Instrument combination	EUSAAR-2 with MAAP	EUSAAR-2 with aethalometer	EUSAAR2 with PSAP	NIOSH-like with aethalo-meter	VDI-2465 with MAAP
Sites	Ispra Montseny Puy de Dôme	Finokalia	Aspvreten Birkenes Vavihill	Harwell	Melpitz
1σ reproducibility of MAC of BC at a wavelength of 637 nm based on harmonized and corrected absorption coefficient and EC mass values. Valid if EUSAAR-2 is defined to be the reference method providing the true EC mass and if total absorption at 637 nm is dominated by BC.	±29%	±43%	±35%	±63%	±57%
Potential maximal systematic difference between reported and true MAC at a wavelength of 637 nm for aerosols that contain light-absorbing organic matter.(Negative value means that the true MAC is smaller than the reported MAC.)	−10%	0%	−30%	0%	−10%
Approximate systematic increase of MAC if the NIOSH-5040 protocol would have been used as reference method for EC mass instead of EUSAAR-2.[a]	+~40%	+~40%	+~40%	+~40%	+~40%
Approximate systematic decrease of MAC if the IMPROVE-A protocol had been used as reference method for EC mass instead of EUSAAR-2.[b]	−~15%	−~15%	−~15%	−~15%	−~15%

[a] Estimated from Piazzalunga et al. (2011) and Maenhaut and Claeys (2012).
[b] Estimated from Piazzalunga et al. (2011) and Wu et al. (2012).

for different aerosol types (WMO, 2016; Collaud Coen et al., 2010; Müller et al., 2011). This results in a 1σ accuracy of $\Delta\sigma_{ap}^{AE} \approx \pm 35\%$ for the corrected absorption coefficients from aethalometers, when combined with unit-to-unit variability, accuracy of the MAAP, which served as a reference, and uncertainty of the AAE of BC applied for wavelength adjustment (Table 5). The 1σ accuracy of corrected absorption coefficients from PSAP measurements is estimated to be $\Delta\sigma_{ap}^{PSAP} \approx \pm 25\%$, where the major uncertainty arises from the instrument-specific PSAP correction factors ($\Delta CF_{PSAP}/CF_{PSAP} \approx \pm 20\%$) applied for correcting the PSAP data towards the MAAP, and from the accuracy of the MAAP itself.

The random errors of total absorption coefficients discussed in the previous paragraph are only valid if light absorption is fully dominated by BC. However, organic matter is known to contribute to light absorption by atmospheric aerosols, particularly in the near-UV wavelength range (e.g. Kirchstetter et al., 2004). Additional errors occur if the ratio of light-absorbing organic matter to BC becomes significant. These errors are systematic and therefore not included in the random errors provided above and separately listed in Table 5. For example, Sandradewi et al. (2008) reported properties of ambient aerosol with a high fraction of organic matter from wood burning. In spite of this, the organic matter contributed only little to total light absorption at a wavelength of 660 nm. We consider 10% interference at a wavelength of 637 nm as an upper limit for the potential light absorption by organic matter in aerosols at the background sites such as those included in the present study. The contribution to absorption by organic matter at 637 nm does a priori not affect the reported aerosol absorption coefficients, which are meant to include the contribution of organic matter. However, it does cause a systematic bias in reported MAC values because we assume that absorption by BC is equal to absorption by the total aerosol for calculating the MAC of BC. Another effect of interference from organic matter is that the true AAE becomes larger than unity as assumed for the wavelength adjustment of Aethalometer and PSAP-ITM data (see Section 2.3.2). Consequently, the true aerosol absorption coefficient at 637 nm will at most be 10% higher or 20% lower than the reported value if inferred from the Aethalometer measurements at 880 nm or the PSAP-ITM measurement at 525 nm. Combining the two systematic interference effects eventually provides true absorption coefficients from BC alone that are at most 0%, 10%, or 30% smaller than the reported total absorption coefficients from Aethalometer, MAAP, or PSAP-ITM measurements, respectively. Note, light absorbing organic matter does not cause a direct systematic error in the absorption coefficient of BC at 637 nm inferred from Aethalometer measurements at 880 nm, as light absorption by such organic matter is negligible at 880 nm wavelength. Additional information on systematic interference from organic matter is provided in Table 5.

The uncertainty of the MAC values, listed in Table 6, is obtained by propagating the uncertainties of the EC mass concentration (Table 4) and the absorption coefficient (Table 5) through Equation (10). The smallest 1σ reproducibility of the MAC of BC is achieved at sites combining MAAP measurements with the EUSAAR-2 thermal-optical protocol and it is estimated to be $\Delta MAC \approx \pm 29\%$. The largest uncertainties were calculated for Melpitz (MAAP/VDI) (±57%), and Harwell (Aethalometer/NIOSH-like), (±63%). These uncertainty estimates are only valid if EUSAAR-2 is defined to be the reference method providing the true EC mass and if the total absorption at 637 nm is dominated by BC. MAC values would be approximately 40% larger if the NIOSH-5040 protocol had been used as reference method for EC mass instead of EUSAAR-2. Light-absorbing organic matter would not affect the MAC values for those sites that operated an Aethalometer. By contrast, the true MAC value of BC would at most be ~10% or ~30% smaller than reported for aerosols containing a large fraction of light-absorbing organic matter and sites that operated a MAAP or PSAP-ITM, respectively.

3. Results and discussion

3.1. Spatial and seasonal variability of m_{EC} and σ_{ap}

Here, we focus on the spatial and seasonal variability of the EC mass concentrations and the absorption coefficients. The annual geometric mean EC mass concentrations differed by more than one order of magnitude between the Puy de Dôme mountain site (0.075 μg m^{-3}) and the polluted regional background site in Ispra (1.1 μg m^{-3}) (Fig. 3a and Table 7). The Scandinavian background sites showed rather low EC burdens (0.084–0.23 μg m^{-3}). Medium EC concentrations were observed at the Mediterranean sites Finokalia and Montseny (0.22–0.26 μg m^{-3}) and at the slightly more

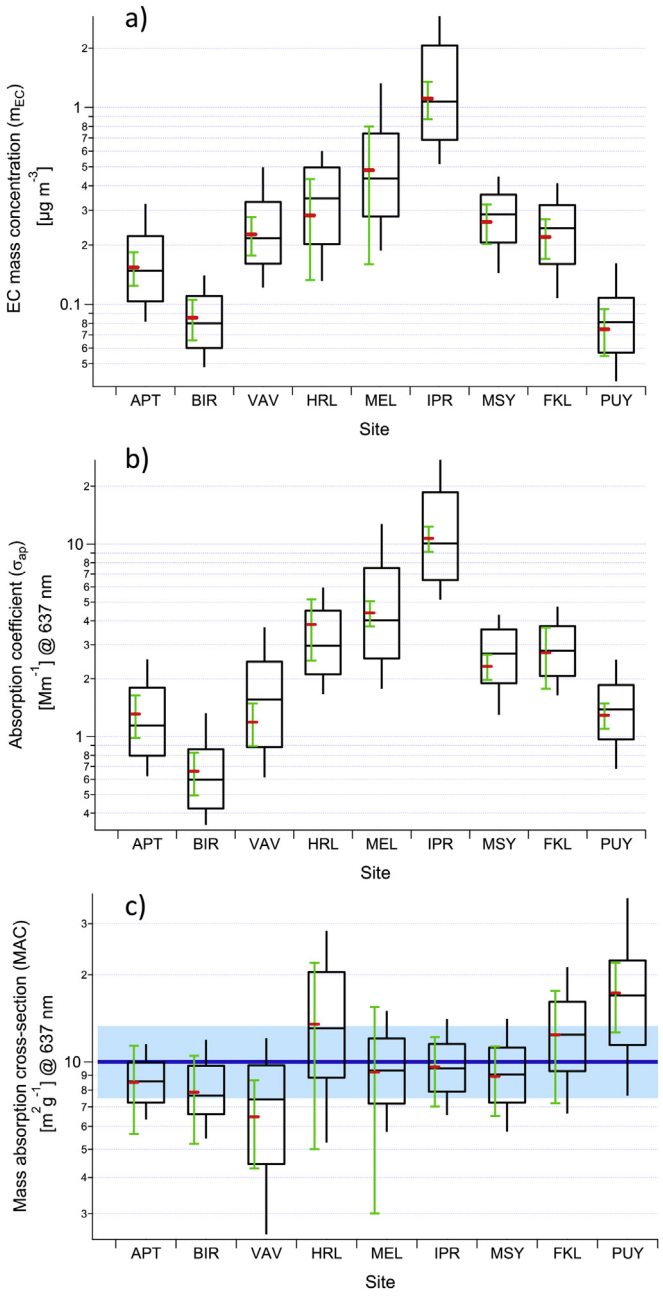

Fig. 3. Box plots showing the 10th, 25th, median, 75th and 90th percentiles (black box and whiskers) as well as geometric mean values (red markers) of a) EUSAAR-2 EC mass concentration, b) absorption coefficient and c) mass absorption cross-section for all nine stations. These statistics are for data averaged over 24 h at all sites, except for the Scandinavian sites (3–7 days). The green error bars indicate the 1σ uncertainties of the geometric mean value, which depend on the applied measurement technique. This uncertainty does not include potential systematic bias arising from e.g. light absorption by organics or from choosing a different thermal-optical protocol as a reference method (see Section 2.3.4 and Tables 4–6 for details). The blue line and shading in panel c indicate the geometric mean ± geometric SD of the annual geometric mean MAC values from all sites. (For interpretation of the references to colour in this figure legend, the reader is referred to the web version of this article.)

polluted British Isles and continental sites Harwell and Melpitz (0.28–0.48 μg m^{-3}). The geometric standard deviations of the annual data-set of EC mass concentrations were between 1.47 and 1.88 for all sites (Table 7). Temporal variability of EC was lowest at the Scandinavian and Mediterranean sites and highest at the Continental as well as British Isles sites, which is mainly attributed

Table 7
Trimmed geometric mean and geometric standard deviation (in brackets) of elemental carbon mass concentration (m_{EC}), for all nine stations. Data are averaged over 24 h at all sites, except for the Scandinavian sites where single filter samples were collected over 3–7 days. Data points below/above the 5th/95th percentile were filtered before statistical analysis.

Elemental carbon mass concentration (m_{EC}) [μg m^{-3}]					
Site	Annual	Winter	Spring	Summer	Autumn
APT	0.15 (1.65)	0.20 (1.68)	0.14 (1.63)	0.14 (1.56)	0.15 (1.51)
BIR	0.084 (1.48)	0.082 (1.66)	0.088 (1.33)	0.077 (1.42)	0.098 (1.48)
FKL	0.22 (1.59)	0.18 (1.65)	0.23 (1.51)	0.28 (1.50)	0.19 (1.55)
HRL	0.28 (1.76)	0.39 (1.59)	0.29 (1.79)	0.22 (1.55)	0.32 (1.77)
IPR	1.11 (1.88)	2.03 (1.61)	0.97 (1.63)	0.63 (1.30)	1.36 (1.76)
MEL	0.48 (1.69)	0.55 (1.71)	0.47 (1.64)	0.32 (1.41)	0.52 (1.68)
MSY	0.26 (1.47)	0.23 (1.48)	0.28 (1.54)	0.29 (1.40)	0.28 (1.43)
PUY	0.075 (1.52)	0.067 (1.55)	0.096 (1.60)	0.073 (1.36)	0.071 (1.35)
VAV	0.227 (1.65)	0.30 (1.69)	0.21 (1.46)	0.17 (1.44)	0.23 (2.01)

to a more pronounced seasonal pattern for the latter (Fig. 4).

The annual geometric mean values of the aerosol absorption coefficient at 637 nm range from 0.66 to 10.7 Mm^{-1} (Table 8). The spatial pattern was very similar to that of the EC mass concentration (Fig. 3b). This is to be expected, if BC is the dominant light absorbing species at 637 nm as argued in Section 2.3.4 because the absorption coefficient is directly related to the EC mass concentration through the MAC value of BC (Equation (10)). One minor difference is that the absorption coefficient was lowest at Birkenes instead of Puy de Dôme, which could reflect a systematic difference in the mean MAC at these two sites or it could simply be caused by experimental uncertainty. The temporal variability of the absorption coefficients was also very similar to that of EC (geom. SD between 1.45 and 1.93), except for Vavihill, where a substantially higher variability of the absorption coefficient (geom. SD 1.93) was observed (Table 8). However, the latter is most likely an artefact caused by very high instrumental noise, rather than reflecting true variability. These results for EC mass concentration and absorption coefficient show a clear spatial pattern with the highest values in Central Europe and distinctly lower values to the North and to the South. This is in agreement with previous studies by Yttri et al. (2007).

The seasonal patterns of the absorption coefficient and EC mass concentration are plotted in Fig. 4a and b. The seasonal patterns of the two quantities are similar as they are linked to each other through the MAC of BC. Thus, we simply discuss the absorption coefficient in the following. The σ_{ap} values observed at the Scandinavian (ASP, BIR and VAV) and central European stations (HRL, IPR and MEL) followed the same pattern, with elevated values in winter/autumn compared to summer/spring. This is likely attributed to a lower polluted boundary layer (PBL) height as well as to higher BC emissions during the heating season. A note is made for the wintertime values observed at Birkenes, as the site experienced unusual meteorological conditions in December 2011, which was exceptionally warm, with a surplus in the average temperature of 8.5 °C and with several aerosol properties untypical for the winter season, which may be explained by reduced emissions from domestic heating and possibly more vertical mixing. Excluding this period from the winter data, i.e. just considering winter 2010 plus January and February 2011, results in considerably higher winter values for the absorption coefficient and EC (square symbols in Fig. 4a and b). An opposite seasonality compared to that in Scandinavia and Central Europe was observed at the Mediterranean sites Finokalia and Montseny, with σ_{ap} values being lowest in winter and highest in summer. At the slightly elevated Montseny site, this is explained by less favorable transport of aerosols to elevated areas during winter, contrasted by regional circulation

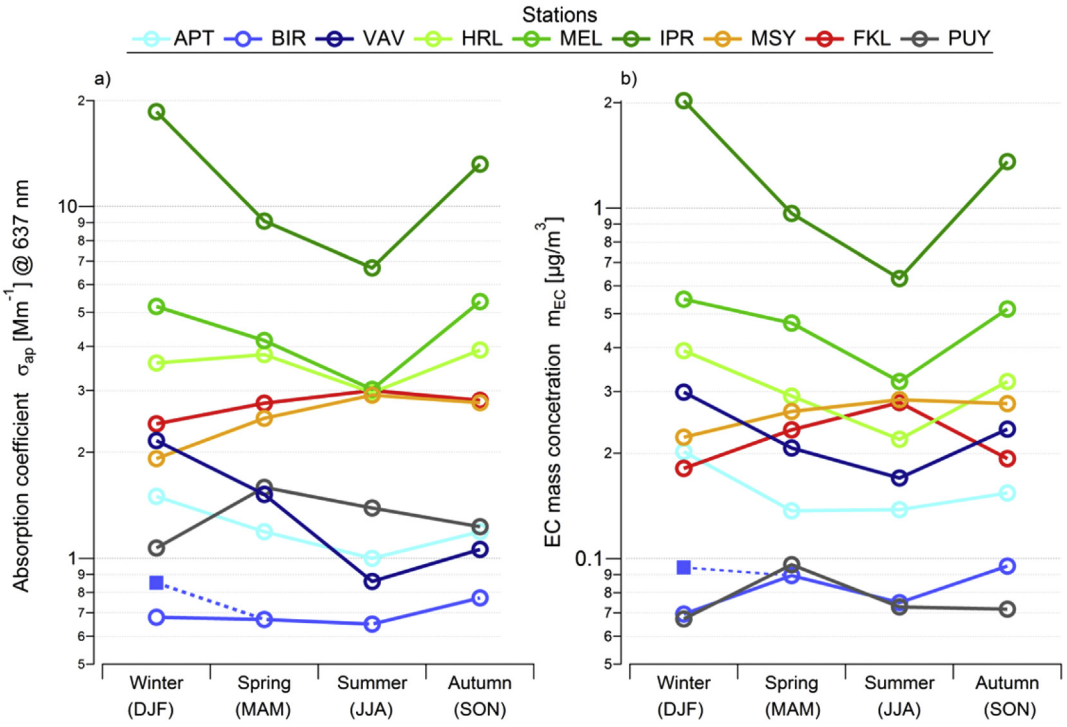

Fig. 4. Seasonal patterns of the geometric mean values for a) absorption coefficients and b) EC mass concentrations. The square marker for Birkenes indicates the geometric mean of all winter data excluding December 2011, which was an outlier from a meteorological point of view, whereas the corresponding circular marker includes December 2011.

Table 8
Trimmed geometric mean and geometric standard deviation (in brackets) of absorption coefficient (σ_{ap}^{637}) for all nine stations. Data are averaged over 24 h at all sites, except for the Scandinavian sites where single filter samples were collected over 3–7 days. Data points below/above the 5th/95th percentile were filtered before statistical analysis.

Absorption coefficient (σ_{ap}^{637}) [Mm^{-1}] @ 637 nm					
Site	Annual	Winter	Spring	Summer	Autumn
APT	1.31 (1.65)	1.50 (1.68)	1.19 (1.65)	1.00 (1.58)	1.19 (1.58)
BIR	0.66 (1.63)	0.67 (1.86)	0.65 (1.52)	0.59 (1.41)	0.68 (1.87)
FKL	2.73 (1.45)	2.41 (1.77)	2.76 (1.30)	3.00 (1.39)	2.81 (1.53)
HRL	3.82 (1.56)	3.59 (1.53)	3.79 (1.43)	2.96 (1.43)	3.91 (1.52)
IPR	10.7 (1.84)	18.6 (1.72)	9.09 (1.63)	6.69 (1.40)	13.2 (1.70)
MEL	4.39 (1.73)	5.20 (1.78)	4.16 (1.63)	3.02 (1.39)	5.37 (1.76)
MSY	2.32 (1.53)	1.92 (1.63)	2.50 (1.52)	2.91 (1.41)	2.77 (1.44)
PUY	1.29 (1.86)	1.07 (1.69)	1.59 (1.66)	1.39 (1.49)	1.23 (1.65)
VAV	1.19 (1.93)	2.16 (1.92)	1.52 (1.79)	0.86 (1.51)	1.06 (1.50)

enabling the accumulation and transport of pollutants from the urbanized coastline to Montseny during summer. The combined effects of rare precipitation, as well as intense agriculture and wildfire events during the warm season, explain the seasonality of σ_{ap} at Finokalia. The seasonal pattern was completely different at the Puy de Dôme mountain station, where σ_{ap} peaked in spring with gradually lower values in summer and autumn, and a minimum in winter. In winter, the Puy de Dôme site is frequently above the PBL, being affected by clean tropospheric air masses. In spring, vertical mixing becomes efficient enough such that the PBL reaches the site, while the wood combustion emissions from domestic heating are still high. The latter fades away in summer, thus explaining the spring maximum (Venzac et al., 2009).

3.2. Spatial variability of the MAC

The overall geometric mean MAC value observed at the 9 European background sites included in the present study was 10.0 m^2 g^{-1} at 637 nm (Fig. 3c). The geometric SD (1.33) of annual geometric mean MAC values at individual stations corresponds to the range from 7.5 to 13.3 m^2 g^{-1} (blue shading in Fig. 3c), while the minimal and maximal observed annual geometric mean values were 6.5 m^2 g^{-1} and 17.3 m^2 g^{-1} (Table 9). The differences between the sites (Table 9) are small in consideration of the experimental uncertainties, which are listed in Table 6 and indicated by the error bars in Fig. 3c.

The results from all stations but Puy de Dôme and Vavihill are in agreement with the overall mean of 10.0 m^2 g^{-1} and within the experimental uncertainty, which can thus be considered to be a representative MAC value of BC at 637 nm with respect to EC mass. It is important to emphasize that systematically higher MAC values would be obtained when using NIOSH-like protocols as a basis for the EC mass measurement instead of EUSAAR-2 (+~40%; Piazzalunga et al., 2011; Maenhaut and Claeys, 2012; see Table 6), whereas a ~15% difference compared to EUSAAR-2 can be expected when using the IMPROVE-A protocol (Karanasiou et al., 2015). Another potential source of systematic errors in the MAC value, which is not included in the error bars of Fig. 3, are interferences in the light absorption measurement from e.g. light-absorbing organic matter. In Table 6, we provide an estimate of the maximum possible systematic bias, obtained by choosing the wavelength dependence of the light absorption coefficient of an ambient aerosol dominated by wood combustion emissions (Sandradewi et al., 2008) as a worst case scenario (see also Section 2.3.4). No interference is expected for the aethalometer based measurements, as the actual measurement is done at 880 nm, where interference is negligible, and extrapolated to 637 nm using an AAE of unity, which is in the range of literature values reported for pure BC particles. For the sites operating a MAAP or PSAP-ITM, which measure at 637 or 525 nm, respectively, the interference can potentially cause a systematic bias of up to around +10% or +30% in the observed MAC of BC. The smallest MAC values were observed at the three Scandinavian sites.

However, the difference from the grand average is within uncertainty, as pointed out above. Likewise, the higher MAC values observed at Harwell are not significantly different due to the additional uncertainties associated with using an aethalometer as well as adjusting EC mass values based on a NIOSH-like protocol to EUSAAR-2 equivalent values. Finokalia is a peculiar case, due to very frequent and strong dust influence, which might contribute to light absorption causing a positive bias. Otherwise, misinterpretation of carbon from carbonates as EC in the thermal-optical analysis would cause a negative bias, due to m_{EC} overestimation. Although the latter might be negligible for fine particulate matter (Querol et al., 2004), it might become severe in case of predominant coarse PM fraction as in the case of dust events (Karanasiou et al., 2015). The MAC values observed during strong dust events were extremely low, which provides clear evidence of negative dust interference. A comparison of days with substantial dust influence (97 days in 2010) with dust-free days in 2010 indicates that the annual geometric mean MAC may have a low bias of ~15% due to dust interference. Accounting for this would move the MAC observed at Finokalia further away from the 10.0 m^2 g^{-1} grand average, however, it would still not differ beyond uncertainty. The MAC values observed at the Puy de Dôme station seem significantly higher than the grand average. Part of this may be explained by more aged BC particles with thicker coatings at this mountain site. However, there is some evidence that the low aerosol loadings frequently encountered at the Puy de Dôme station may have caused a low bias in the EC mass measurements and thus a high bias in the MAC values, which is not accounted for in our uncertainty analysis. Indeed, previous studies at the high-alpine site Jungfraujoch, Switzerland, reported values close to 10.0 m^2 g^{-1} (Cozic et al., 2008; Liu et al., 2010).

Generally, the literature values for the MAC of BC listed in Table 1 are in the same ballpark as our grand average, though with considerably more variability than the spatial variability observed in our study. Genberg et al. (2013) also presented MAC values for the Melpitz, Aspreveten, Birkenes and Vavihill stations, which are also included in our study. Their MAC value reported for Melpitz is substantially lower than ours, which can be explained by the fact that they directly used the VDI-based EC mass concentrations, whereas we adjusted them to EUSAAR-2 equivalent values with the correction factors provided in Figure S1 and in Table 3. The MAC values reported by Genberg et al. (2013) for the Scandinavian sites are substantially higher than our results, which can be explained by the fact that we adjusted the PSAP-ITM based absorption coefficient measurements to MAAP equivalent values using the correction factors listed in Table 3.

In summary, the extensive intercomparison and harmonization efforts within the ACTRIS network made it possible to achieve a homogeneous long-term data-set from many background sites across Europe, which reveals only limited spatial variability of the mean MAC values. We recommend a MAC value of 10.0 m^2 g^{-1} at 637 nm as best-estimate value for Europe, whenever a fixed MAC of BC is required for conversion of EUSAAR-2 based (or equivalent) EC mass concentrations to corresponding absorption coefficients, e.g. in model simulations, or for conversion from measured absorption coefficients to equivalent black carbon (eBC) mass concentrations. Potential systematic dependence of the MAC on the aerosol mixing state will be addressed in Section 3.4.

3.3. Temporal variability and seasonal cycles of the MAC

In the previous section, we showed that the annual MAC-values exhibit little spatial variability across Europe. Here we investigate the temporal variability and seasonal patterns (Fig. 5 and Table 7). The trimmed geometric standard deviation of all observed MAC values was not exceeding 1.34 for the three sites Aspvreten, Birkenes and Ispra. Such small variability is rather surprising, given the fact that a substantial fraction of it can be attributed to the random noise of single EC measurements, which have a repeatability that is hardly better than around ±10–20% (Cavalli et al., 2016). Thus, the true MAC value likely has little temporal variability at these sites, which also is consistent with little seasonal variability; i.e. within the uncertainty. The observed MAC at Vavihill, the third Scandinavian background site, appeared much more variable in time. However, this is most likely an artefact from an uncommonly poor signal-to-noise ratio in the absorption coefficient measurements (see also Sect. 3.1). In combination with poor counting statistics, it would be purely speculative to interpret the apparent seasonal pattern observed for this site in Fig. 5. The temporal variability observed at the Montseny site was in the medium range (geom. SD = 1.65) but without any significant seasonal pattern. Melpitz exhibited surprisingly small temporal variability, given the fact that the EC mass measurements were made with the VDI thermal protocol and adjusted to EUSAAR-2 equivalent EC mass values (see Section 2.3.1). The higher MAC observed in autumn is not significant, because the adjustment is tainted with considerable uncertainty and potential systematic seasonal bias (Figure S1 and Table 6). A mid-range temporal variability and higher values in autumn were observed at the Finokalia site. However, this may simply reflect differences between weak and strong dust interferences that affect the MAC values at this site (Section 3.2). The MAC values observed at the Harwell and Puy de Dôme site exhibited much higher temporal variability and apparent seasonal patterns. However, this is not statistically significant due to the relatively small number of samples and increased instrumental variability associated with using a different thermal-optical protocol (Harwell) and possible issues with very low aerosol concentrations (Puy de Dôme), respectively. In summary, the temporal variability of the observed MAC values was rather small, indicating a good repeatability of the measurements, whereas no statistically significant seasonal pattern could be observed for any of the sites.

3.4. Dependence of the MAC on BC mixing state

Formation of a light-scattering coating around a BC core leads to enhanced light absorption, often referred to as the lensing effect. This is theoretically expected (e.g. Fuller et al., 1999; Nessler et al., 2005; Bond and Bergstrom, 2006; Lack and Cappa, 2010) and has later been observed in laboratory and field experiments (Schwarz et al., 2008a; Lack et al., 2009; Shiraiwa et al., 2010). Here we investigate whether evidence for light absorption enhancement by a light-scattering coating around the BC core is observed. The available datasets do not allow quantifying the mixing state and coating thickness of BC-containing particles. Therefore, we use the mass ratio of non-absorbing matter (NAM) to EC as a proxy for the thickness of coatings around the BC cores. Some correlation between this proxy and the average coatings of the BC-containing particles can be expected for the following reasons: A substantial fraction of BC is typically externally mixed close to major sources of BC (e.g. Laborde et al., 2013; Swietlicki et al., 2008), where BC mass fractions in the aerosol are relatively high (Hueglin et al., 2005) and thus NAM to EC relatively low. Additionally the formation of secondary NAM from gas phase precursors during the transport of air masses away from major BC sources results in coating acquisition by BC particles through condensation (e.g. Engelhart et al., 2012; Dahlkötter et al., 2014) and an increase of the NAM to EC mass ratio.

The NAM to EC mass ratio was calculated with the EC mass concentrations from the thermal-optical analyses and we defined NAM as the sum of particulate organic matter, nitrate and non-sea-salt sulfate (nss-sulfate). The components included in NAM

typically account for a major fraction of the submicron particulate matter and they are mainly of secondary origin, thus supporting the use of the NAM to EC ratio as a proxy for BC coating thickness (sea salt sulfate is not included in NAM as it is expected to be externally mixed to a large extent). The mass concentration of organic matter was inferred by multiplying the OC mass concentration obtained from the thermal-optical measurements with a factor of 1.6 (Turpin et al., 2000; Pio et al., 2007). Inorganic ions were measured by ion chromatography of water extracts from quartz filter samples. nss-sulfate is calculated as the difference between total measured sulfate mass and estimated sea salt sulfate mass, where the sea salt sulfate mass is set equal to one quarter of the total measured sodium mass (Pio et al., 2007). This approach might suffer from some bias due to the contribution of mineral dust to the sodium mass (Alastuey et al., 2016).

The chemical composition data required to calculate NAM as defined above are only available for the five stations Birkenes, Harwell, Ispra, Melpitz and Montseny and only for 2010. More details on the data availability are given in the supplementary material (Table S2). Annual geometric mean mass concentrations of EC as well as nss-sulfate, nitrate and organic matter are listed in Table 10, while mass fractions of these components with respect to the sum of EC plus NAM are shown in Fig. 6a. Except for the Harwell site, organic matter constitutes the largest fraction with 48%–61%. EC is always a minor component (2–11%). Nitrate and nss-sulfate are also minor components at most sites. At Harwell, nitrate (44%) and nss-sulfate (29%) are the major components of the NAM, while organic matter represents 25%.

The observed dependence of the MAC on the BC coating thickness proxy is shown in Fig. 6b. The result for the Birkenes site (blue line with markers), where no dependence of the MAC on the coating thickness proxy is observed, is an unexplained exception. For the other 4 sites, a clear trend of increasing MAC of BC with increasing value of the coating thickness proxy is observed from MAC values between 5.7 and 9.0 $m^2\ g^{-1}$ at NAM/EC < 10 to values between 9.0 and 15.7 $m^2\ g^{-1}$ at NAM/EC between 30 and 40. The grey shading in Fig. 6b frames the approximate range of physically reasonable MAC values, which was obtained as follows. Concentric-spheres core-shell morphology was assumed for the BC core and the coating such that Mie theory could be applied. Three different BC core diameters of 100, 150 and 200 nm were used, which covers the typical range where BC mass size distributions peak when expressed as a function of BC core mass equivalent diameter (Schwarz et al., 2008b; Laborde et al., 2013). The index of refraction of the BC core was assumed to be 1.88 + 0.8i (Liu et al., 2015), which was already used during a European study and is in the range of expected values according to Bond and Bergstrom (2006). Three different indices of refraction (1.45+0i, 1.50+0i and 1.55+0i), which represent typical values of organic and inorganic species present in atmospheric aerosols, were used for the coating (e. g. Hess et al., 1998; Bond et al., 2006; Dinar et al., 2008; Moffet and Prather, 2009). The core-shell diameter ratio was either set to unity to obtain the minimal possible MAC of bare BC cores, or set to values > 10 to obtain the maximal possible MAC in the range where the lensing effect is fully saturated, i.e. where a further coating thickness increase does not change the MAC any further (e.g. Nessler et al., 2005). The minimal and maximal MAC for a given set of parameters were calculated with all possible combinations of BC core diameter and coating index of refraction, and the average of it was chosen as approximation for the minimum (6.0 $m^2\ g^{-1}$) and maximum (14.5 $m^2\ g^{-1}$) possible MAC values at a wavelength of 637 nm. These estimates of the upper and lower limits for possible MAC values are consistent with previous literature on theoretically calculated MAC values. Most observations in Fig. 6b fall into the physical boundaries, except for very high NAM to EC ratios. However, the latter data points are likely biased high due to a substantial and asymmetric contribution from outliers in the EC mass concentration and/or absorption coefficient data. The results shown in Fig. 6b provide evidence that the lensing effect results in increased MAC values, as theoretically expected, and that variability of the average coating thickness of BC explains part of the temporal variability of the MAC values. However, the actual magnitude of the lensing effect could be smaller than implied by Fig. 6b, as it cannot be excluded that experimental artefacts cause part of the correlation between MAC and NAM/EC. Nevertheless, the fit line in Fig. 6b, i.e. $MAC_{637nm}\ [m^2\ g^{-1}] = 0.13\ m^2\ g^{-1} \bullet (NAM/EC) + 7.25\ m^2\ g^{-1}$, could serve as a basis for model-based sensitivity analyses to assess the potential importance of the lensing effect on the radiative forcing through light-absorption by BC. The axis intercept of the fit line, i.e. 7.25 $m^2\ g^{-1}$, represents the approximate MAC of externally mixed BC at a wavelength of 637 nm. This is a rather uncertain extrapolation of our data set. Nonetheless, it is in agreement with MAC values previously reported for urban aerosols (e.g. Hitzenberger et al., 2006).

The EC mass concentration appears as the denominator in the equation to calculate both the MAC value and the NAM to EC ratio. Therefore, random noise in the EC mass measurement does also cause a positive correlation between MAC and NAM/EC. This effect, assessed and discussed in the supplementary material, caused most likely only a minor fraction of the observed dependence of the MAC on NAM/EC.

Imperfect correction for multiple scattering within the filter matrix of the absorption instruments may potentially cause an apparent lensing effect as multiple scattering could be increased by deposition of light-scattering particulate matter. This applies particularly to the Harwell data, where an aethalometer was applied, whereas it is unlikely to cause an apparent absorption enhancement by a factor of ~2 for the Melpitz, Ispra and Montseny sites, where a MAAP was used (though Melpitz has considerably larger uncertainty in EC mass measurements, due to the seasonality of the harmonization factor). We do not know whether the exceptional behavior of MAC versus NAM to EC mass ratio observed for the Birkenes data, where the absorption was measured with a PSAP-ITM instrument, reflects a true difference in aerosol properties.

Interference from light-absorbing organic particulate matter would also cause an apparent lensing effect, however the estimated contribution to the total aerosol light absorption at wavelength larger than 637 nm has been shown to be less than 10% (Lack et al., 2012; Feng et al., 2013; Liu et al., 2015). Accordingly, only a minor fraction of the MAC increase seen in the bottom panel of Fig. 6b can potentially be caused by such interference.

Table 9
Trimmed geometric mean and geometric standard deviation (in brackets) of mass absorption cross-section (MAC^{637}) for all nine stations. Data are averaged over 24 h at all sites, except for the Scandinavian sites where single filter samples were collected over 3–7 days. Data points below/above the 5th/95th percentile were filtered before statistical analysis.

Mass absorption cross-section (MAC^{637}) [$m^2\ g^{-1}$] @ 637 nm					
Site	Annual	Winter	Spring	Summer	Autumn
APT	8.51 (1.26)	8.38 (1.22)	9.10 (1.27)	8.41 (1.24)	8.17 (1.30)
BIR	7.86 (1.34)	8.09 (1.33)	7.59 (1.30)	8.12 (1.27)	7.71 (1.43)
FKL	12.4 (1.56)	15.1 (1.75)	11.1 (1.47)	10.9 (1.55)	15.1 (1.45)
HRL	13.5 (1.82)	8.87 (1.84)	14.9 (1.75)	15.9 (1.71)	15.1 (1.56)
IPR	9.61 (1.34)	9.31 (1.35)	9.03 (1.30)	10.9 (1.35)	9.34 (1.30)
MEL	9.23 (1.45)	8.22 (1.47)	8.74 (1.47)	9.5 (1.38)	11.3 (1.36)
MSY	8.92 (1.65)	8.29 (1.82)	8.97 (1.64)	9.73 (1.55)	8.73 (1.57)
PUY	17.3 (1.71)	13.4 (1.62)	16.5 (1.70)	19.9 (1.68)	19.8 (1.73)
VAV	6.47 (1.81)	7.04 (1.87)	7.23 (1.61)	4.85 (1.71)	4.20 (2.39)

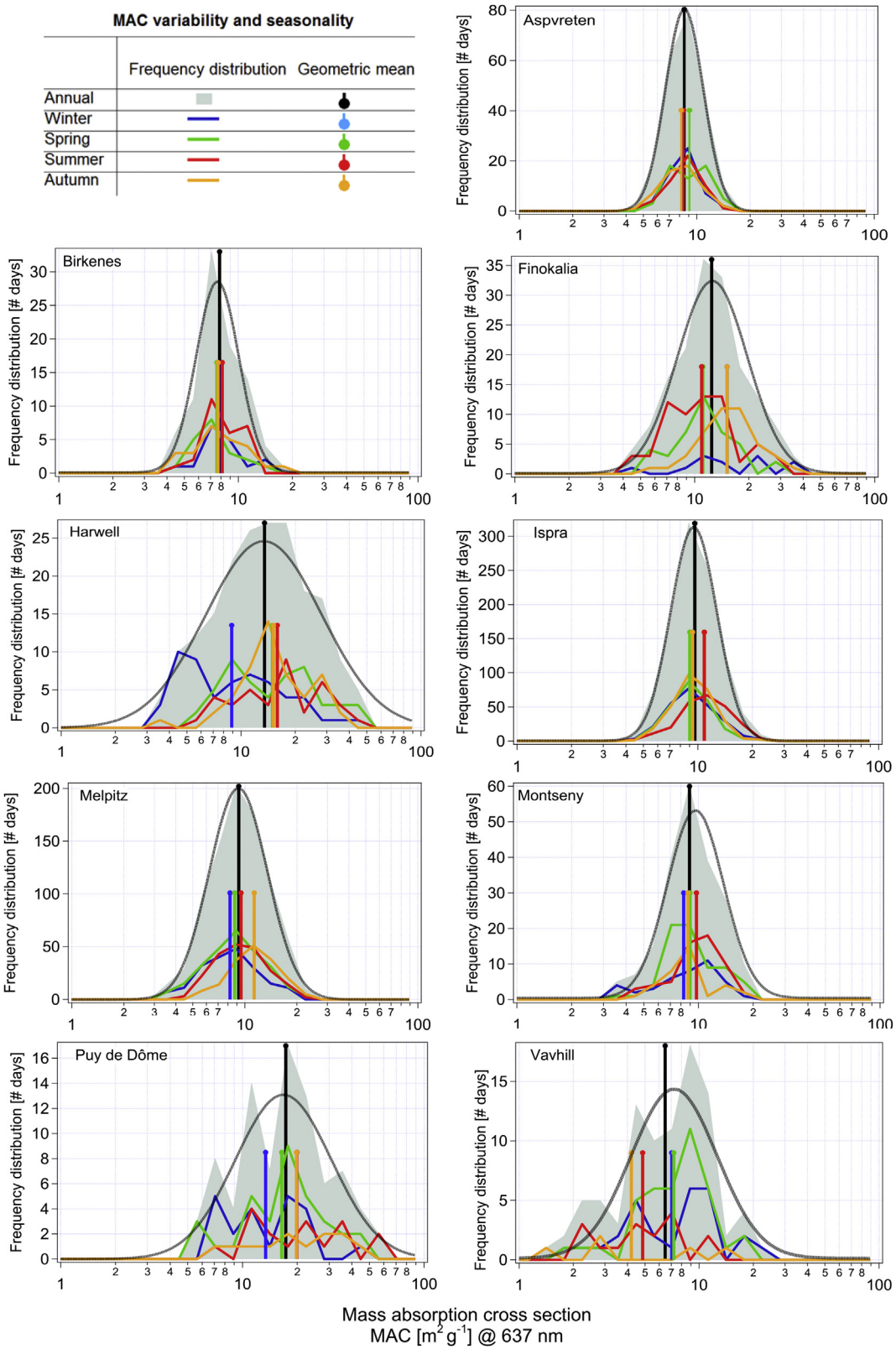

Fig. 5. Frequency distribution of mass absorption cross-section (MAC) of black carbon for the whole multi-annual measurement period (grey surface) and corresponding geometric mean MAC (black sticks). Seasonal data are shown as colored lines and sticks. Lognormal fitting of MAC values is shown as black dashed curves.

So far we have argued that a substantial part of the observed MAC enhancement through the internal mixing of BC with light-scattering particulate matter is likely reflecting a true lensing effect rather than just measurement artefacts and that it is essentially consistent with theoretical expectations. Several previous experimental investigations of the lensing effect using

Table 10
Mass concentration of carbonaceous (OM and EC) and inorganic (non-sea salt sulfate and nitrate) particulate matter. Annual geometric mean with geometric SD in parentheses for 2010.

Mass concentration: geometric mean (geometric SD) [μg m^{-3}]				
	EC	OM	nss-sulfate	Nitrate
BIR	0.10 (1.71)	1.18 (1.66)	0.15 (2.68)	0.55 (2.27)
HRL	0.30 (2.34)	3.16 (1.71)	1.05 (2.39)	5.49 (12.0)
IPR	1.03 (2.35)	5.84 (3.12)	0.52 (3.43)	1.20 (6.74)
MEL	0.52 (2.54)	4.62 (2.02)	0.65 (2.36)	3.15 (4.97)
MSY	0.20 (1.88)	2.59 (1.52)	0.31 (2.79)	0.83 (2.19)

laboratory-generated and ambient aerosols also reported a substantial increase of light absorption by BC caused by coating acquisition, with maximal enhancement factors reaching up to ~2 (Schnaiter et al., 2005; Knox et al., 2009; Shiraiwa et al., 2010). By contrast, other studies on ambient aerosols report enhancement by as little as ~7% (Cappa et al., 2012; Lan et al., 2013). Our study provides another piece of evidence that the lensing effect can cause substantial MAC enhancement for internally mixed atmospheric BC particles.

4. Conclusions

In this study, we have presented the spatial and seasonal variability of the light absorption coefficient, the EC mass concentration and the corresponding BC mass absorption cross section (MAC) from long-term measurements at 9 rural background sites of the ACTRIS research infrastructure network across Europe. Homogeneity of data-sets was ensured by harmonization of all involved methods and instruments during extensive intercomparison exercises at the European Center for Aerosol Calibration.

The observed MAC values do not have distinct seasonal patterns at individual sites and annual values were equal within uncertainty across almost all locations. The geometric mean of the annual geometric means from each site is 10.0 m^2 g^{-1} (geometric SD = 1.33 resulting in a range of 7.5–13.3 m^2 g^{-1}) at a wavelength of 637 nm. Consequently, we recommend this MAC value of BC, which is valid for EC mass defined through the EUSAAR-2 thermal-optical protocol, as best-estimate value for European background sites. However, absolute uncertainties of the reported MAC values remain as high as ± 30–70% due to the lack of appropriate reference methods. For example applying different thermal-optical protocols would potentially result in systematically different MAC values. This

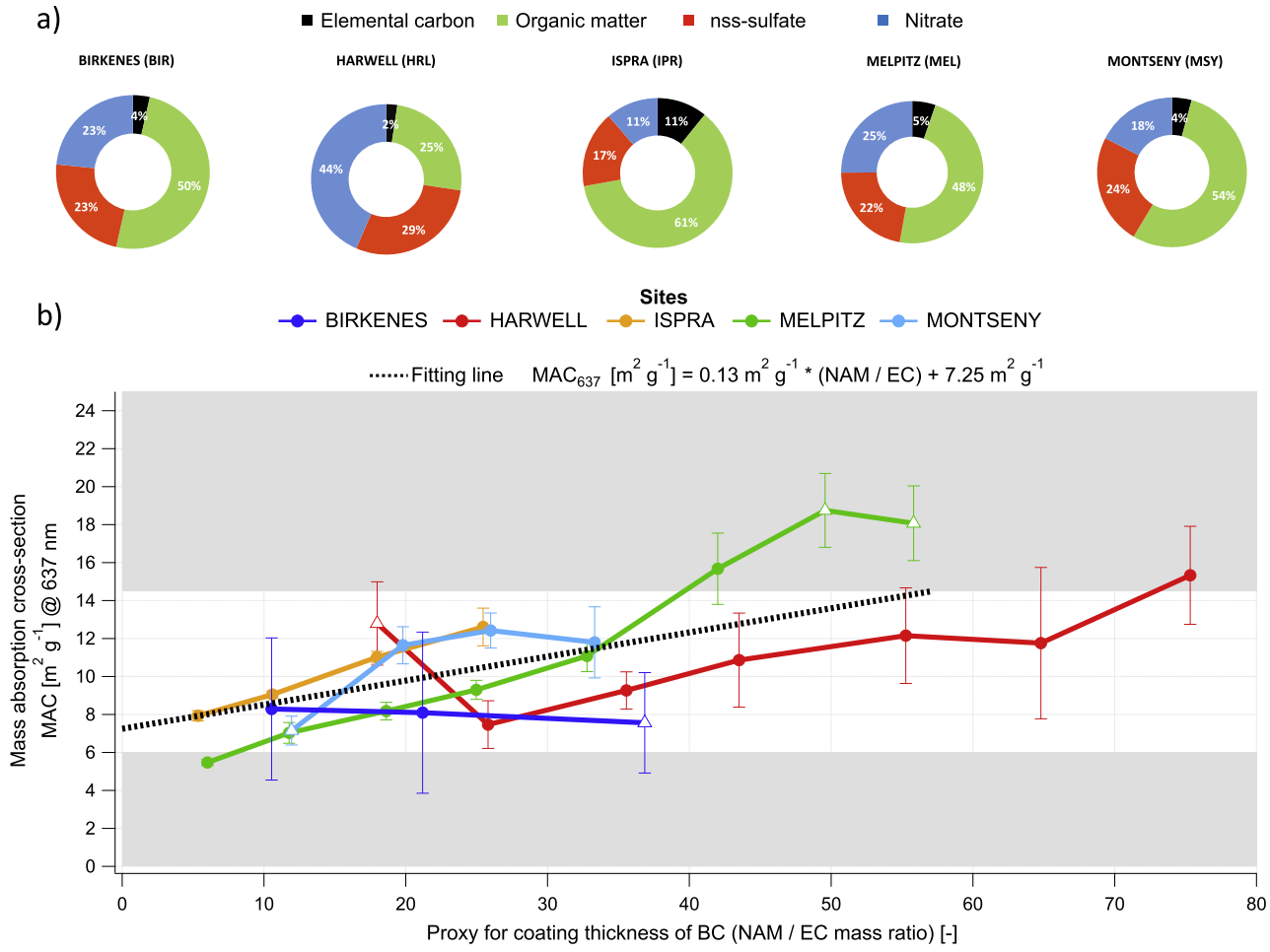

Fig. 6. a) Annual mean mass fractions of major aerosol components (organic matter, sulfate, nitrate and elemental carbon) used as input for the BC mixing state proxy. b) Dependence of the MAC on the proxy for the coating thickness, defined as the mass ratio of non-absorbing matter (NAM) to elemental carbon (EC). Individual data points were grouped into bins with different NAM to EC mass ratios. The circular markers show the mean MAC value and the mean NAM to EC mass ratio of all data points falling into the corresponding bin. Averages based on 5–10 data points only are drawn as empty triangles instead of circles. Error bars represent the standard error of the mean value. The grey shading frames the approximate range of physically reasonable MAC values calculated using Mie theory. Experimental results outside this range are likely biased due to a substantial and asymmetric contribution from outliers in the EC mass concentration and/or absorption coefficient data.

comprehensive data-set also provides evidence that the lensing effect likely causes part of the observed variability of the MAC value, i.e. that internal mixing of BC with other aerosol components enhances the light absorption by BC.

The observed absorption coefficients and EC mass concentrations exhibit distinct seasonal patterns. These patterns are almost equal for the absorption coefficient and EC at a given site, while they differ substantially between different locations. The former is a direct consequence of the fact that the MAC value exhibits only limited temporal variability without significant seasonal patterns.

Acknowledgments

The research leading to these results has received funding from the European Union Seventh Framework Programme (ACTRIS, FP7/2007-2013, grant agreement no. 262254). ACTRIS-2 is a European Project supported by the European Commission Horizon 2020 Research and Innovation Framework Programme (ACTRIS-2, H2020-INFRAIA-2014-2015, grant agreement no. 654109). This work was also supported by grants from Labex OSUG@2020 (PhD investissements d'avenir – ANR10 LABX56) and from the European Research Council (ERC-CoG 615922-BLACARAT).

Appendix A. Supplementary data

Supplementary data related to this article can be found at http://dx.doi.org/10.1016/j.atmosenv.2016.09.035.

References

Alastuey, A., Querol, X., Aas, W., Lucarelli, F., Perez, N., Moreno, T., Cavalli, F., Areskoug, H., Balan, V., Catrambone, M., Ceburnis, D., Cerro, J.C., Conil, S., Gevorgyan, L., Hueglin, C., Imre, K., Jafrezzo, J.-L., Leeson, S.R., Mihalopoulos, N., Mitosinkova, M., Pey, J., Putaud, J.-P., Riffault, V., Ripoll, A., Sciare, J., Sellegri, K., Spinder, G., Yttri, K.E., 2016. Geochemistry of PM10 over Europe during the EMEP intensive measurement periods in summer 2012 and winter 2013. Atmos. Chem. Phys. Discuss. 1–37. http://dx.doi.org/10.5194/acp-2016-42.

Baumgardner, D., Popovicheva, O., Allan, J., Bernardoni, V., Cao, J., Cavalli, F., Cozic, J., Diapouli, E., Eleftheriadis, K., Genberg, P.J., Gonzalez, C., Gysel, M., John, A., Kirchstetter, T.W., Kuhlbusch, T.A.J., Laborde, M., Lack, D., Müller, T., Niessner, R., Petzold, A., Piazzalunga, A., Putaud, J.P., Schwarz, J., Sheridan, P., Subramanian, R., Swietlicki, E., Valli, G., Vecchi, R., Viana, M., 2012. Soot reference materials for instrument calibration and intercomparisons: a workshop summary with recommendations. Atmos. Meas. Tech. 5 (8), 1869–1887. http://dx.doi.org/10.5194/amt-5-1869-2012.

Birch, M.E., Cary, R.A., 1996. Elemental carbon-based method for monitoring occupational exposures to particulate diesel exhaust. Aerosol. Sci. Technol. 25 (3), 221–241. http://dx.doi.org/10.1080/02786829608965393.

Bond, T.C., Bergstrom, R.W., 2006. Light absorption by carbonaceous particles: an investigative review. Aerosol. Sci. Technol. 40 (1), 27–67. http://dx.doi.org/10.1080/02786820500421521.

Bond, T.C., Anderson, T.L., Campbell, D., 1999. Calibration and intercomparison of filter-based measurements of visible light absorption by aerosols. Aerosol. Sci. Technol. 30 (6), 582–600. http://dx.doi.org/10.1080/027868299304435.

Bond, T.C., Habib, G., Bergstrom, R.W., 2006. Limitations in the enhancement of visible light absorption due to mixing state. J. Geophys. Res. Atmos. 111 (D20), D20211. http://dx.doi.org/10.1029/2006JD007315.

Bond, T.C., Doherty, S.J., Fahey, D.W., Forster, P.M., Berntsen, T., DeAngelo, B.J., Flanner, M.G., Ghan, S., Kärcher, B., Koch, D., Kinne, S., Kondo, Y., Quinn, P.K., Sarofim, M.C., Schultz, M.G., Schulz, M., Venkataraman, C., Zhang, H., Zhang, S., Bellouin, N., Guttikunda, S.K., Hopke, P.K., Jacobson, M.Z., Kaiser, J.W., Klimont, Z., Lohmann, U., Schwarz, J.P., Shindell, D., Storelvmo, T., Warren, S.G., Zender, C.S., 2013. Bounding the role of black carbon in the climate system: a scientific assessment. J. Geophys. Res. Atmos. 118 (11), 5380–5552. http://dx.doi.org/10.1002/jgrd.50171.

Cachier, H., Bremond, M.-P., Buat-Ménard, P., 1989. Determination of atmospheric soot carbon with a simple thermal method. Tellus B 41B (3), 379–390. http://dx.doi.org/10.1111/j.1600-0889.1989.tb00316.x.

Cappa, C.D., Onasch, T.B., Massoli, P., Worsnop, D.R., Bates, T.S., Cross, E.S., Davidovits, P., Hakala, J., Hayden, K.L., Jobson, B.T., Kolesar, K.R., Lack, D.A., Lerner, B.M., Li, S.-M., Mellon, D., Nuaaman, I., Olfert, J.S., Petäjä, T., Quinn, P.K., Song, C., Subramanian, R., Williams, E.J., Zaveri, R.A., 2012. Radiative absorption enhancements due to the mixing state of atmospheric black carbon. Science 337 (6098), 1078–1081. http://dx.doi.org/10.1126/science.1223447.

Cavalli, F., Viana, M., Yttri, K.E., Genberg, J., Putaud, J.-P., 2010. Toward a standardised thermal-optical protocol for measuring atmospheric organic and elemental carbon: the EUSAAR protocol. Atmos. Meas. Tech. 3 (1), 79–89. http://dx.doi.org/10.5194/amt-3-79-2010.

Cavalli, F., Alastuey, A., Areskoug, H., Cech, J., Ceburnis, D., Genberg, J., Harrison, R.M., Jaffrezo, J.L., Kiss, G., Mihalopoulos, N., Perez, N., Quincey, P., Schwarz, J., Sellegri, K., Spindler, G., Theodosi, C., Yttri, K.E., Aas, W., Putaud, J.P., 2016. A European aerosol phenomenology-4: harmonized concentrations of carbonaceous aerosol at 10 regional background sites across Europe. Atmos. Environ. (submitted for publication).

Chiappini, L., Verlhac, S., Aujay, R., Maenhaut, W., Putaud, J.P., Sciare, J., Jaffrezo, J.L., Liousse, C., Galy-Lacaux, C., Alleman, L.Y., Panteliadis, P., Leoz, E., Favez, O., 2014. Clues for a standardised thermal-optical protocol for the assessment of organic and elemental carbon within ambient air particulate matter. Atmos. Meas. Tech. 7 (6), 1649–1661. http://dx.doi.org/10.5194/amt-7-1649-2014.

Chow, J.C., Watson, J.G., Pritchett, L.C., Pierson, W.R., Frazier, C.A., Purcell, R.G., 1993. The dri thermal/optical reflectance carbon analysis system: description, evaluation and applications in U.S. Air quality studies. Atmos. Environ. Part Gen. Top. 27 (8), 1185–1201. http://dx.doi.org/10.1016/0960-1686(93)90245-T.

Chow, J.C., Watson, J.G., Chen, L.-W.A., Chang, M.C.O., Robinson, N.F., Trimble, D., Kohl, S., 2007. The IMPROVE_A temperature protocol for thermal/optical carbon analysis: maintaining consistency with a long-term database. J. Air Waste Manag. Assoc. 57 (9), 1014–1023. http://dx.doi.org/10.3155/1047-3289.57.9.1014.

Collaud Coen, M., Weingartner, E., Apituley, A., Ceburnis, D., Fierz-Schmidhauser, R., Flentje, H., Henzing, J.S., Jennings, S.G., Moerman, M., Petzold, A., Schmid, O., Baltensperger, U., 2010. Minimizing light absorption measurement artifacts of the Aethalometer: evaluation of five correction algorithms. Atmos. Meas. Tech. 3 (2), 457–474. http://dx.doi.org/10.5194/amt-3-457-2010.

Cozic, J., Verheggen, B., Weingartner, E., Crosier, J., Bower, K.N., Flynn, M., Coe, H., Henning, S., Steinbacher, M., Henne, S., Collaud Coen, M., Petzold, A., Baltensperger, U., 2008. Chemical composition of free tropospheric aerosol for PM1 and coarse mode at the high alpine site Jungfraujoch. Atmos. Chem. Phys. 8 (2), 407–423. http://dx.doi.org/10.5194/acp-8-407-2008.

Dahlkötter, F., Gysel, M., Sauer, D., Minikin, A., Baumann, R., Seifert, P., Ansmann, A., Fromm, M., Voigt, C., Weinzierl, B., 2014. The Pagami Creek smoke plume after long-range transport to the upper troposphere over Europe – aerosol properties and black carbon mixing state. Atmos. Chem. Phys. 14 (12), 6111–6137. http://dx.doi.org/10.5194/acp-14-6111-2014.

Dinar, E., Riziq, A.A., Spindler, C., Erlick, C., Kiss, G., Rudich, Y., 2008. The complex refractive index of atmospheric and model humic-like substances (HULIS) retrieved by a cavity ring down aerosol spectrometer (CRD-AS). Faraday Discuss. 137, 279–295 discussion 297–318.

Dod, R.L., Rosen, H., Novakov, T., 1979. Optico-thermal analysis of the carbonaceous fraction of aerosol particles. In: Atmospheric Aerosol Research Annual Report 1977–1978 (No. LBL 8696). Lawrence Berkeley Laboratory, pp. 2–10.

Engelhart, G.J., Hennigan, C.J., Miracolo, M.A., Robinson, A.L., Pandis, S.N., 2012. Cloud condensation nuclei activity of fresh primary and aged biomass burning aerosol. Atmos. Chem. Phys. 12 (15), 7285–7293. http://dx.doi.org/10.5194/acp-12-7285-2012.

Feng, Y., Ramanathan, V., Kotamarthi, V.R., 2013. Brown carbon: a significant atmospheric absorber of solar radiation? Atmos. Chem. Phys. 13 (17), 8607–8621. http://dx.doi.org/10.5194/acp-13-8607-2013.

Fierce, L., Riemer, N., Bond, T.C., 2015. Explaining variance in black carbon's aging timescale. Atmos. Chem. Phys. 15 (6), 3173–3191. http://dx.doi.org/10.5194/acp-15-3173-2015.

Fuller, K.A., Malm, W.C., Kreidenweis, S.M., 1999. Effects of mixing on extinction by carbonaceous particles. J. Geophys. Res. Atmos. 104 (D13), 15941–15954. http://dx.doi.org/10.1029/1998JD100069.

Genberg, J., Denier van der Gon, H.A.C., Simpson, D., Swietlicki, E., Ceburnis, D., Fiebig, M., Hansson, H.C., Harrison, R.M., Jennings, S.G., Saarikoski, S., Spindler, G., Visschedijk, A.J.H., Wiedensohler, A., Yttri, K.E., Bergström, R., 2013. Light-absorbing carbon in Europe – measurement and modelling, with a focus on residential wood combustion emissions. Atmos. Chem. Phys. 13 (17), 8719–8738. http://dx.doi.org/10.5194/acp-13-8719-2013.

Hansen, A.D.A., Rosen, H., Novakov, T., 1984. The aethalometer — an instrument for the real-time measurement of optical absorption by aerosol particles. Sci. Total Environ. 36, 191–196. http://dx.doi.org/10.1016/0048-9697(84)90265-1.

Henne, S., Brunner, D., Folini, D., Solberg, S., Klausen, J., Buchmann, B., 2010. Assessment of parameters describing representativeness of air quality in-situ measurement sites. Atmos. Chem. Phys. 10 (8), 3561–3581. http://dx.doi.org/10.5194/acp-10-3561-2010.

Herich, H., Hueglin, C., Buchmann, B., 2011. A 2.5 year's source apportionment study of black carbon from wood burning and fossil fuel combustion at urban and rural sites in Switzerland,. Atmos. Meas. Tech. 4 (7), 1409–1420. http://dx.doi.org/10.5194/amt-4-1409-2011.

Hess, M., Koepke, P. and Schult, I.: Optical properties of aerosols and clouds: the software package OPAC, Bull. Am. Meteorol. Soc., 79(5), 831–844, doi:10.1175/1520-0477(1998)079<0831:OPOAAC>2.0.CO;2, 1998.

Hitzenberger, R., Petzold, A., Bauer, H., Ctyroky, P., Pouresmaeil, P., Laskus, L., Puxbaum, H., 2006. Intercomparison of thermal and optical measurement methods for elemental carbon and black carbon at an urban location. Environ. Sci. Technol. 40 (20), 6377–6383. http://dx.doi.org/10.1021/es051228v.

Hueglin, C., Gehrig, R., Baltensperger, U., Gysel, M., Monn, C., Vonmont, H., 2005. Chemical characterisation of PM2.5, PM10 and coarse particles at urban, near-city and rural sites in Switzerland. Atmos. Environ. 39, 637–651. http://

dx.doi.org/10.1016/j.atmosenv.2004.10.027.
Huntzicker, J.J., Johnson, R.L., Shah, J.J., Cary, R.A., 1982. Analysis of organic and elemental carbon in ambient aerosols by a thermal-optical method. In: Wolff, G.T., Klimisch, R.L. (Eds.), Particulate Carbon. Springer, US, pp. 79–88 [online] Available from: http://link.springer.com/chapter/10.1007/978-1-4684-4154-3_6 (Accessed 23 November 2015).
Jacobson, M.Z., 2001. Strong radiative heating due to the mixing state of black carbon in atmospheric aerosols. Nature 409 (6821), 695–697.
Johnson, R.L., Huntzicker, J.J., 1979. Analysis of volatilizable and elemental carbon in ambient aerosols. In: Novakov, T. (Ed.), Proceedings: Carbonaceous Particles in the Atmosphere. Lawrence Berkeley Laboratory, Berkelely, California, pp. 10–13.
Karanasiou, A., Minguillón, M.C., Viana, M., Alastuey, A., Putaud, J.-P., Maenhaut, W., Panteliadis, P., Močnik, G., Favez, O., Kuhlbusch, T.A.J., 2015. Thermal-optical analysis for the measurement of elemental carbon (EC) and organic carbon (OC) in ambient air a literature review. Atmos. Meas. Tech. Discuss. 8 (9), 9649–9712. http://dx.doi.org/10.5194/amtd-8-9649-2015.
Kirchstetter, T.W., Novakov, T., Hobbs, P.V., 2004. Evidence that the spectral dependence of light absorption by aerosols is affected by organic carbon. J. Geophys. Res. Atmos. 109 (D21), D21208. http://dx.doi.org/10.1029/2004JD004999.
Knox, A., Evans, G.J., Brook, J.R., Yao, X., Jeong, C.-H., Godri, K.J., Sabaliauskas, K., Slowik, J.G., 2009. Mass absorption cross-section of ambient black carbon aerosol in relation to chemical age. Aerosol. Sci. Technol. 43 (6), 522–532. http://dx.doi.org/10.1080/02786820902777207.
Koch, D., Schulz, M., Kinne, S., McNaughton, C., Spackman, J.R., Balkanski, Y., Bauer, S., Berntsen, T., Bond, T.C., Boucher, O., Chin, M., Clarke, A., De Luca, N., Dentener, F., Diehl, T., Dubovik, O., Easter, R., Fahey, D.W., Feichter, J., Fillmore, D., Freitag, S., Ghan, S., Ginoux, P., Gong, S., Horowitz, L., Iversen, T., Kirkevåg, A., Klimont, Z., Kondo, Y., Krol, M., Liu, X., Miller, R., Montanaro, V., Moteki, N., Myhre, G., Penner, J.E., Perlwitz, J., Pitari, G., Reddy, S., Sahu, L., Sakamoto, H., Schuster, G., Schwarz, J.P., Seland, Ø., Stier, P., Takegawa, N., Takemura, T., Textor, C., van Aardenne, J.A., Zhao, Y., 2009. Evaluation of black carbon estimations in global aerosol models. Atmos. Chem. Phys. 9 (22), 9001–9026. http://dx.doi.org/10.5194/acp-9-9001-2009.
Krecl, P., Ström, J., Johansson, C., 2007. Carbon content of atmospheric aerosols in a residential area during the wood combustion season in Sweden. Atmos. Environ. 41 (33), 6974–6985. http://dx.doi.org/10.1016/j.atmosenv.2007.06.025.
Laborde, M., Crippa, M., Tritscher, T., Jurányi, Z., Decarlo, P.F., Temime-Roussel, B., Marchand, N., Eckhardt, S., Stohl, A., Baltensperger, U., Prévôt, A.S.H., Weingartner, E., Gysel, M., 2013. Black carbon physical properties and mixing state in the European megacity Paris. Atmos. Chem. Phys. 13 (11), 5831–5856. http://dx.doi.org/10.5194/acp-13-5831-2013.
Lack, D.A., Cappa, C.D., 2010. Impact of brown and clear carbon on light absorption enhancement, single scatter albedo and absorption wavelength dependence of black carbon. Atmos. Chem. Phys. 10, 4207–4220.
Lack, D.A., Langridge, J.M., 2013. On the attribution of black and brown carbon light absorption using the Ångström exponent. Atmos. Chem. Phys. 13 (20), 10535–10543. http://dx.doi.org/10.5194/acp-13-10535-2013.
Lack, D.A., Cappa, C.D., Cross, E.S., Massoli, P., Ahern, A.T., Davidovits, P., Onasch, T.B., 2009. Absorption enhancement of coated absorbing aerosols: validation of the photo-acoustic technique for measuring the enhancement. Aerosol. Sci. Technol. 43 (10), 1006–1012. http://dx.doi.org/10.1080/02786820903117932.
Lack, D.A., Langridge, J.M., Bahreini, R., Cappa, C.D., Middlebrook, A.M., Schwarz, J.P., 2012. Brown carbon and internal mixing in biomass burning particles. Proc. Natl. Acad. Sci. 109 (37), 14802–14807. http://dx.doi.org/10.1073/pnas.1206575109.
Lan, Z.-J., Huang, X.-F., Yu, K.-Y., Sun, T.-L., Zeng, L.-W., Hu, M., 2013. Light absorption of black carbon aerosol and its enhancement by mixing state in an urban atmosphere in South China. Atmos. Environ. 69, 118–123. http://dx.doi.org/10.1016/j.atmosenv.2012.12.009.
Liousse, C., Cachier, H., Jennings, S.G., 1993. Optical and thermal measurements of black carbon aerosol content in different environments: variation of the specific attenuation cross-section, sigma (σ). Atmos. Environ. Part Gen. Top. 27 (8), 1203–1211. http://dx.doi.org/10.1016/0960-1686(93)90246-U.
Liu, D., Flynn, M., Gysel, M., Targino, A., Crawford, I., Bower, K., Choularton, T., Jurányi, Z., Steinbacher, M., Hüglin, C., Curtius, J., Kampus, M., Petzold, A., Weingartner, E., Baltensperger, U., Coe, H., 2010. Single particle characterization of black carbon aerosols at a tropospheric alpine site in Switzerland. Atmos. Chem. Phys. 10 (15), 7389–7407. http://dx.doi.org/10.5194/acp-10-7389-2010.
Liu, S., Aiken, A.C., Gorkowski, K., Dubey, M.K., Cappa, C.D., Williams, L.R., Herndon, S.C., Massoli, P., Fortner, E.C., Chhabra, P.S., Brooks, W.A., Onasch, T.B., Jayne, J.T., Worsnop, D.R., China, S., Sharma, N., Mazzoleni, C., Xu, L., Ng, N.L., Liu, D., Allan, J.D., Lee, J.D., Fleming, Z.L., Mohr, C., Zotter, P., Szidat, S., Prévôt, A.S.H., 2015. Enhanced light absorption by mixed source black and brown carbon particles in UK winter. Nat. Commun. 6, 8435. http://dx.doi.org/10.1038/ncomms9435.
Maenhaut, W., Claeys, M., 2012. EC=OC Analyses 2010–2011, Final report, Study for the Vlaamse Milieumaatschappij (VMM), afdeling Meetnetten en Onderzoek. Order number: LUC/2010/EC/OC, 25 July 2011. Flemish Environment Agency.
Martins, J.V., Artaxo, P., Liousse, C., Reid, J.S., Hobbs, P.V., Kaufman, Y.J., 1998. Effects of black carbon content, particle size, and mixing on light absorption by aerosols from biomass burning in Brazil. J. Geophys. Res. 103 (D24), 32041–32050. http://dx.doi.org/10.1029/98JD02593.
Moffet, R.C., Prather, K.A., 2009. In-situ measurements of the mixing state and optical properties of soot with implications for radiative forcing estimates. Proc. Natl. Acad. Sci. 106 (29), 11872–11877. http://dx.doi.org/10.1073/pnas.0900040106.
Moosmüller, H., Chakrabarty, R.K., Arnott, W.P., 2009. Aerosol light absorption and its measurement: a review. J. Quant. Spectrosc. Radiat. Transf. 110 (11), 844–878. http://dx.doi.org/10.1016/j.jqsrt.2009.02.035.
Moteki, N., Kondo, Y., Miyazaki, Y., Takegawa, N., Komazaki, Y., Kurata, G., Shirai, T., Blake, D.R., Miyakawa, T., Koike, M., 2007. Evolution of mixing state of black carbon particles: aircraft measurements over the western Pacific in March 2004. Geophys. Res. Lett. 34 (11), L11803. http://dx.doi.org/10.1029/2006GL028943.
Müller, T., Henzing, J.S., de Leeuw, G., Wiedensohler, A., Alastuey, A., Angelov, H., Bizjak, M., Collaud Coen, M., Engström, J.E., Gruening, C., Hillamo, R., Hoffer, A., Imre, K., Ivanow, P., Jennings, G., Sun, J.Y., Kalivitis, N., Karlsson, H., Komppula, M., Laj, P., Li, S.-M., Lunder, C., Marinoni, A., Martins dos Santos, S., Moerman, M., Nowak, A., Ogren, J.A., Petzold, A., Pichon, J.M., Rodriquez, S., Sharma, S., Sheridan, P.J., Teinilä, K., Tuch, T., Viana, M., Virkkula, A., Weingartner, E., Wilhelm, R., Wang, Y.Q., 2011. Characterization and intercomparison of aerosol absorption photometers: result of two intercomparison workshops. Atmos. Meas. Tech. 4 (2), 245–268. http://dx.doi.org/10.5194/amt-4-245-2011.
Myhre, G., Samset, B.H., Schulz, M., Balkanski, Y., Bauer, S., Berntsen, T.K., Bian, H., Bellouin, N., Chin, M., Diehl, T., Easter, R.C., Feichter, J., Ghan, S.J., Hauglustaine, D., Iversen, T., Kinne, S., Kirkevåg, A., Lamarque, J.-F., Lin, G., Liu, X., Lund, M.T., Luo, G., Ma, X., van Noije, T., Penner, J.E., Rasch, P.J., Ruiz, A., Seland, ø, Skeie, R.B., Stier, P., Takemura, T., Tsigaridis, K., Wang, P., Wang, Z., Xu, L., Yu, H., Yu, F., Yoon, J.-H., Zhang, K., Zhang, H., Zhou, C., 2013. Radiative forcing of the direct aerosol effect from AeroCom Phase II simulations. Atmos. Chem. Phys. 13 (4), 1853–1877. http://dx.doi.org/10.5194/acp-13-1853-2013.
Nessler, R., Weingartner, E., Baltensperger, U., 2005. Effect of humidity on aerosol light absorption and its implications for extinction and the single scattering albedo illustrated for a site in the lower free troposphere. J. Aerosol. Sci. 36 (8), 958–972. http://dx.doi.org/10.1016/j.jaerosci.2004.11.012.
Nordmann, S., Birmili, W., Weinhold, K., Müller, K., Spindler, G., Wiedensohler, A., 2013. Measurements of the mass absorption cross section of atmospheric soot particles using Raman spectroscopy. J. Geophys. Res. Atmos. 118 (21), 12,075–12,085. http://dx.doi.org/10.1002/2013JD020021.
Ogren, J.A., 2010. Comment on “calibration and intercomparison of filter-based measurements of visible light absorption by aerosols”. Aerosol. Sci. Technol. 44 (8), 589–591. http://dx.doi.org/10.1080/02786826.2010.482111.
Pandolfi, M., Cusack, M., Alastuey, A., Querol, X., 2011. Variability of aerosol optical properties in the Western Mediterranean Basin. Atmos. Chem. Phys. 11 (15), 8189–8203. http://dx.doi.org/10.5194/acp-11-8189-2011.
Pandolfi, M., Ripoll, A., Querol, X., Alastuey, A., 2014. Climatology of aerosol optical properties and black carbon mass absorption cross section at a remote high-altitude site in the western Mediterranean Basin. Atmos. Chem. Phys. 14 (12), 6443–6460. http://dx.doi.org/10.5194/acp-14-6443-2014.
Petzold, A., Schönlinner, M., 2004. Multi-angle absorption photometry—a new method for the measurement of aerosol light absorption and atmospheric black carbon. J. Aerosol. Sci. 35 (4), 421–441. http://dx.doi.org/10.1016/j.jaerosci.2003.09.005.
Petzold, A., Schloesser, H., Sheridan, P.J., Arnott, W.P., Ogren, J.A., Virkkula, A., 2005. Evaluation of multiangle absorption photometry for measuring aerosol light absorption. Aerosol. Sci. Technol. 39 (1), 40–51. http://dx.doi.org/10.1080/027868290901945.
Petzold, A., Ogren, J.A., Fiebig, M., Laj, P., Li, S.-M., Baltensperger, U., Holzer-Popp, T., Kinne, S., Pappalardo, G., Sugimoto, N., Wehrli, C., Wiedensohler, A., Zhang, X.-Y., 2013. Recommendations for reporting “black carbon” measurements. Atmos. Chem. Phys. 13 (16), 8365–8379. http://dx.doi.org/10.5194/acp-13-8365-2013.
Piazzalunga, A., Belis, C., Bernardoni, V., Cazzuli, O., Fermo, P., Valli, G., Vecchi, R., 2011. Estimates of wood burning contribution to PM by the macro-tracer method using tailored emission factors. Atmos. Environ. 45 (37), 6642–6649. http://dx.doi.org/10.1016/j.atmosenv.2011.09.008.
Pio, C.A., Legrand, M., Oliveira, T., Afonso, J., Santos, C., Caseiro, A., Fialho, P., Barata, F., Puxbaum, H., Sanchez-Ochoa, A., Kasper-Giebl, A., Gelencsér, A., Preunkert, S., Schock, M., 2007. Climatology of aerosol composition (organic versus inorganic) at nonurban sites on a west-east transect across Europe. J. Geophys. Res. Atmos. 112 (D23), D23S02. http://dx.doi.org/10.1029/2006JD008038.
Putaud, J.-P., Raes, F., Van Dingenen, R., Brüggemann, E., Facchini, M.-C., Decesari, S., Fuzzi, S., Gehrig, R., Hüglin, C., Laj, P., Lorbeer, G., Maenhaut, W., Mihalopoulos, N., Müller, K., Querol, X., Rodriguez, S., Schneider, J., Spindler, G., ten Brink, H., Tørseth, K., Wiedensohler, A., 2004. A European aerosol phenomenology—2: chemical characteristics of particulate matter at kerbside, urban, rural and background sites in Europe. Atmos. Environ. 38 (16), 2579–2595. http://dx.doi.org/10.1016/j.atmosenv.2004.01.041.
Querol, X., Alastuey, A., Ruiz, C.R., Artiñano, B., Hansson, H.C., Harrison, R.M., Buringh, E., ten Brink, H.M., Lutz, M., Bruckmann, P., Straehl, P., Schneider, J., 2004. Speciation and origin of PM10 and PM2.5 in selected European cities. Atmos. Environ. 38 (38), 6547–6555. http://dx.doi.org/10.1016/j.atmosenv.2004.08.037.
Querol, X., Alastuey, A., Viana, M., Moreno, T., Reche, C., Minguillón, M.C., Ripoll, A., Pandolfi, M., Amato, F., Karanasiou, A., Pérez, N., Pey, J., Cusack, M., Vázquez, R., Plana, F., Dall'Osto, M., de la Rosa, J., Sánchez de la Campa, A., Fernández-Camacho, R., Rodríguez, S., Pio, C., Alados-Arboledas, L., Titos, G., Artíñano, B., Salvador, P., García Dos Santos, S., Fernández Patier, R., 2013. Variability of

carbonaceous aerosols in remote, rural, urban and industrial environments in Spain: implications for air quality policy. Atmos. Chem. Phys. 13 (13), 6185–6206. http://dx.doi.org/10.5194/acp-13-6185-2013.

Reche, C., Querol, X., Alastuey, A., Viana, M., Pey, J., Moreno, T., Rodríguez, S., González, Y., Fernández-Camacho, R., de la Rosa, J., Dall'Osto, M., Prévôt, A.S.H., Hueglin, C., Harrison, R.M., Quincey, P., 2011. New considerations for PM, Black Carbon and particle number concentration for air quality monitoring across different European cities. Atmos. Chem. Phys. 11 (13), 6207–6227. http://dx.doi.org/10.5194/acp-11-6207-2011.

Riemer, N., West, M., Zaveri, R., Easter, R., 2010. Estimating black carbon aging time-scales with a particle-resolved aerosol model. J. Aerosol. Sci. 41 (1), 143–158. http://dx.doi.org/10.1016/j.jaerosci.2009.08.009.

Sandradewi, J., Prévôt, A.S.H., Szidat, S., Perron, N., Alfarra, M.R., Lanz, V.A., Weingartner, E., Baltensperger, U., 2008. Using aerosol light absorption measurements for the quantitative determination of wood burning and traffic emission contributions to particulate matter. Environ. Sci. Technol. 42 (9), 3316–3323.

Schnaiter, M., Linke, C., Möhler, O., Naumann, K.-H., Saathoff, H., Wagner, R., Schurath, U., Wehner, B., 2005. Absorption amplification of black carbon internally mixed with secondary organic aerosol. J. Geophys. Res. Atmos. 110 (D19), D19204. http://dx.doi.org/10.1029/2005JD006046.

Schulz, M., Textor, C., Kinne, S., Balkanski, Y., Bauer, S., Berntsen, T., Berglen, T., Boucher, O., Dentener, F., Guibert, S., Isaksen, I.S.A., Iversen, T., Koch, D., Kirkevåg, A., Liu, X., Montanaro, V., Myhre, G., Penner, J.E., Pitari, G., Reddy, S., Seland, Ø., Stier, P., Takemura, T., 2006. Radiative forcing by aerosols as derived from the AeroCom present-day and pre-industrial simulations. Atmos. Chem. Phys. 6 (12), 5225–5246. http://dx.doi.org/10.5194/acp-6-5225-2006.

Schwarz, J.P., Spackman, J.R., Fahey, D.W., Gao, R.S., Lohmann, U., Stier, P., Watts, L.A., Thomson, D.S., Lack, D.A., Pfister, L., Mahoney, M.J., Baumgardner, D., Wilson, J.C., Reeves, J.M., 2008a. Coatings and their enhancement of black carbon light absorption in the tropical atmosphere. J. Geophys. Res. Atmos. 113 (D3), D03203. http://dx.doi.org/10.1029/2007JD009042.

Schwarz, J.P., Gao, R.S., Spackman, J.R., Watts, L.A., Thomson, D.S., Fahey, D.W., Ryerson, T.B., Peischl, J., Holloway, J.S., Trainer, M., Frost, G.J., Baynard, T., Lack, D.A., de Gouw, J.A., Warneke, C., Del Negro, L.A., 2008b. Measurement of the mixing state, mass, and optical size of individual black carbon particles in urban and biomass burning emissions. Geophys. Res. Lett. 35 (13), L13810. http://dx.doi.org/10.1029/2008GL033968.

Shiraiwa, M., Kondo, Y., Iwamoto, T., Kita, K., 2010. Amplification of light absorption of black carbon by organic coating. Aerosol. Sci. Technol. 44 (1), 46–54. http://dx.doi.org/10.1080/02786820903357686.

Slowik, J.G., Cross, E.S., Han, J.-H., Davidovits, P., Onasch, T.B., Jayne, J.T., Williams, L.R., Canagaratna, M.R., Worsnop, D.R., Chakrabarty, R.K., Moosmüller, H., Arnott, W.P., Schwarz, J.P., Gao, R.-S., Fahey, D.W., Kok, G.L., Petzold, A., 2007. An inter-comparison of instruments measuring black carbon content of soot particles. Aerosol. Sci. Technol. 41 (3), 295–314. http://dx.doi.org/10.1080/02786820701197078.

Swietlicki, E., Hansson, H.-C., Hämeri, K., Svenningsson, B., Massling, A., McFiggans, G., McMurry, P.H., Petäjä, T., Tunved, P., Gysel, M., Topping, D., Weingartner, E., Baltensperger, U., Rissler, J., Wiedensohler, A., Kulmala, M., 2008. Hygroscopic properties of submicrometer atmospheric aerosol particles measured with H-TDMA instruments in various environments - a review. Tellus B 60, 432–469. http://dx.doi.org/10.1111/j.1600-0889.2008.00350.x.

Turpin, B.J., Saxena, P., Andrews, E., 2000. Measuring and simulating particulate organics in the atmosphere: problems and prospects. Atmos. Environ. 34 (18), 2983–3013. http://dx.doi.org/10.1016/S1352-2310(99)00501-4.

Venzac, H., Sellegri, K., Villani, P., Picard, D., Laj, P., 2009. Seasonal variation of aerosol size distributions in the free troposphere and residual layer at the puy de Dôme station, France. Atmos. Chem. Phys. 9 (4), 1465–1478. http://dx.doi.org/10.5194/acp-9-1465-2009.

Vignati, E., Karl, M., Krol, M., Wilson, J., Stier, P., Cavalli, F., 2010. Sources of uncertainties in modelling black carbon at the global scale. Atmos. Chem. Phys. 10 (6), 2595–2611. http://dx.doi.org/10.5194/acp-10-2595-2010.

Weingartner, E., Saathoff, H., Schnaiter, M., Streit, N., Bitnar, B., Baltensperger, U., 2003. Absorption of light by soot particles: determination of the absorption coefficient by means of aethalometers. J. Aerosol. Sci. 34 (10), 1445–1463. http://dx.doi.org/10.1016/S0021-8502(03)00359-8.

WMO, 2016. Aerosol Measurements Procedures Guidelines and Recomendations, second ed. World Meterological Organization, Geneva.

Wu, C., Ng, W.M., Huang, J., Wu, D., Yu, J.Z., 2012. Determination of elemental and organic carbon in PM2.5 in the Pearl River delta region: inter-instrument (Sunset vs. DRI Model 2001 Thermal/optical carbon analyzer) and inter-protocol comparisons (IMPROVE vs. ACE-Asia protocol). Aerosol. Sci. Technol. 46 (6), 610–621. http://dx.doi.org/10.1080/02786826.2011.649313.

Yttri, K.E., Aas, W., Bjerke, A., Cape, J.N., Cavalli, F., Ceburnis, D., Dye, C., Emblico, L., Facchini, M.C., Forster, C., Hanssen, J.E., Hansson, H.C., Jennings, S.G., Maenhaut, W., Putaud, J.P., Tørseth, K., 2007. Elemental and organic carbon in PM10: a one year measurement campaign within the European Monitoring and Evaluation Programme EMEP. Atmos. Chem. Phys. 7 (22), 5711–5725. http://dx.doi.org/10.5194/acp-7-5711-2007.

Yttri, K.E., Dye, C., Braathen, O.-A., Simpson, D., Steinnes, E., 2009. Carbonaceous aerosols in Norwegian urban areas. Atmos. Chem. Phys. 9 (6), 2007–2020. http://dx.doi.org/10.5194/acp-9-2007-2009.